

**RHIC Multi-Year Beam Use Request
For Runs VI – VIII**

The STAR Collaboration

October 12, 2005

Table of Contents

| | |
|---|----|
| Executive Summary | 3 |
| 1. Progress from Runs IV and V | 5 |
| 1.1 Recent Results on Relativistic Heavy Ions | 6 |
| 2. Proposed Beam Use for Run VI (2005-2006) | 15 |
| 2.1 Changes to the STAR Detector Configuration for Run VI | 17 |
| 2.2 Proposed Gluon Polarization Measurement with Longitudinal Polarization | 19 |
| 2.3 Recent Results and Status | 24 |
| 2.3.1 Inclusive Jet Cross Sections and Asymmetries | 24 |
| 2.3.2 Inclusive π^0 Production | 27 |
| 2.4 Worldwide Competition to Determine Gluon Polarization | 31 |
| 2.5 Transverse Spin Physics Goals | 33 |
| 2.6 Low Energy Au+Au Collisions: the Onset of Hydrodynamic Behavior | 37 |
| 3. Proposal for RHIC Run VII (2006-2007) | 38 |
| 3.1 d+Au: the Search for Gluon Saturation (Color Glass Condensate) in Heavy Nuclei | 39 |
| 3.2 p+p: Reference Data for the CGC; Progress in Mapping the Helicity Preference of Gluons as a Function of x Bjorken | 42 |
| 4.0 Proposal for RHIC Run VIII (2007-2008) | 43 |
| 5. Collaboration Readiness | 45 |

**RHIC Multi-Year Beam Use Request
For Runs VI - VIII
The STAR Collaboration**

October 12, 2005

Executive Summary

The STAR Collaboration, in order to achieve its spin and relativistic heavy ion physics goals on a timescale consistent with intense international interest and competition in these areas, as well as to utilize RHIC beams effectively taking full advantage of planned improvements in machine and detector capability as a function of time, makes the following 3 year beam use proposal:

| Run | Energy | System | Goal |
|------|--|---|--|
| VI | $\sqrt{s} = 200 \text{ GeV}$ $\sqrt{s} = 200 \text{ GeV}$ $\sqrt{s_{NN}} = 19.6, 31 \text{ GeV}$ | $p\uparrow p\uparrow$ $p\rightarrow p\rightarrow$ Au + Au | 10 pb^{-1} sampled 20 pb^{-1} sampled 1 + 1 weeks* (10M + 10M evts) |
| VII | $\sqrt{s_{NN}} = 200 \text{ GeV}$ $\sqrt{s} = 200 \text{ GeV}$ | d + Au $p\rightarrow p\rightarrow$ | 11 weeks 10 weeks |
| VIII | $\sqrt{s_{NN}} = 200 \text{ GeV}$ $\sqrt{s} = 200 \text{ GeV}$ | Au + Au $p\rightarrow p\rightarrow$ | 15 weeks 6 weeks |

* Contingent on achieving spin physics integrated luminosity targets

The primary physics goals of the proposed program are:

- Run VI Place a world-class constraint on gluon polarization in the proton, Δg
Delineate the roles of parton orbital motion/transversity in creating the transverse single spin asymmetry (A_N) observed for inclusive forward π^0 production
First significant measurement of Sivers effect asymmetry in di-jet production
- Run VII Decisive test of existence of the Color Glass Condensate in relativistic heavy nuclei
Detailed mapping of the x dependence of gluon polarization in the proton, $\Delta g(x)$
- Run VIII Precision tests of the properties of quark-gluon matter
Search for chiral symmetry restoration

The STAR Collaboration feels strongly that the proposed plan is optimal to make the most efficient use of RHIC beam time for timely progress in determining the properties of the Quark-Gluon Plasma, searching for the Color Glass Condensate, and measuring the gluon polarization in the proton, $\Delta g(x)$.

Specifically, since upgrades planned or in progress will improve the performance of the detector significantly by Run VIII (in some cases by an order of magnitude), it is most effective to defer the next long Au+Au run until these upgrades are substantially complete, making a strong advance in the interim on measuring $\Delta g(x)$ and searching for the CGC in Runs VI and VII. In addition, the long p+p run proposed for Run VI will provide C-AD the opportunity to continue machine developments, such as the commissioning of the cold snake in the AGS, to improve the luminosity and polarization further. These developments are essential in order to achieve the ultimate STAR goal for 200 GeV running – a direct measurement of the momentum-dependence of the gluon polarization, $\Delta g(x)$, over a broad x range via the γ +jet channel.

The near-term upgrades planned by STAR are a Forward Meson Spectrometer, a barrel TOF detector, DAQ1000 upgrade, and a micro-vertex detector. For Run VIII STAR expects to have the complete FMS (Run VII), the complete DAQ1000 upgrade, half of the TOF barrel detector, and a prototype micro-vertex detector. Longer term, a forward tracking upgrade is planned for $\sqrt{s} = 500$ GeV polarized p+p running to insure accurate charge sign determination for electrons (positrons) from W^\pm decay. Such decays will be used to study the flavor decomposition of quark/anti-quark polarization in the proton.

1. Report on Progress from Runs IV and V (2004 – 2005)

For the heavy ion program, the first priority for beam use by STAR in the 2004-2005 run (Run V) was the accumulation of approximately 50 million minimum bias Cu+Cu collisions at $\sqrt{s_{NN}} = 200$ GeV, along with a sample of rare triggers corresponding to 1-2 nb^{-1} of recorded luminosity. A performance-based goal of running for 1-2 weeks at $\sqrt{s_{NN}} = 62.4$ GeV was also proposed contingent on machine performance allowing the full energy goals to be met sufficiently early. The purpose of these studies was to obtain experimental “control data” by varying the system size to test the dependence of high p_T particle suppression, elliptic flow, and heavy flavor production on gluon density and pressure in the early stage of the collision. A specific goal was to test the predicted L^2 dependence of partonic energy loss in a system substantially smaller than AuAu for which the suppression was nevertheless expected to be sufficiently large it could be reliably observed based on the suppression observed for AuAu collisions with comparable $N_{part} \sim 115$ (equivalent to 30-40% central for AuAu).

For the spin program, a dataset expected to result in a significant measurement of the gluon helicity preference in the proton by studying the double spin asymmetry (A_{LL}) for inclusive π^0 and jet production was proposed. The highest priority was to obtain a sample of rare triggers corresponding to 7 pb^{-1} of recorded luminosity at longitudinal polarization P of 40%, corresponding to a recorded Figure of Merit (FOM) of $P^4L = 180 \text{ nb}^{-1}$. A secondary goal, subject to successful completion of the longitudinal spin measurement, was to sample $> 4 \text{ pb}^{-1}$ with beams of transversely polarized protons ($P > 40\%$) to study the large transverse single spin asymmetry (SSA) observed earlier¹ for forward π^0 production and assess its origin in terms of possible effects of orbital motion (Sivers effect), Collins effect, or twist-3 quark-gluon correlations.

As seen in Table 1, the primary goals for Run V were all substantially met.

Table I

| Energy (GeV) | $\sqrt{s_{NN}}$ | Trigger | System | Acquired | Goal |
|--------------|-----------------|------------------------|--------------------|-----------------------------------|--|
| 200 | | Minimum Bias | Cu+Cu | 65 M events | > 50 M |
| 200 | | Rare (BEMC High Tower) | Cu+Cu | 1.05 nb^{-1} recorded | 1-2 nb^{-1} recorded |
| 62.4 | | Minimum Bias | Cu+Cu | 37 M events | 1-2 weeks |
| 22 | | Minimum Bias | Cu+Cu | 3.5 M events | Not requested |
| 200 | | Rare | p+p (longitudinal) | FOM~156 nb^{-1} recorded | 7 pb^{-1} @ 40% P FOM = 180 nb^{-1} |
| 200 | | Rare | p+p (transverse) | Few % of goal | 4 pb^{-1} @ 40% P |
| 410 | | Rare | p+p (transverse) | ~ 6 hrs of data | Not requested |

1.1 Recent Results on Relativistic Heavy Ions

The analysis of the heavy ion data taken in Run V is ongoing, and preliminary results from this dataset were presented at Quark Matter 2005. As seen in Fig. 1, suppression of high p_T charged particles in Cu+Cu is significant and consistent with that of peripheral Au+Au data at the same number of participants (N_{part}). The greater precision possible in controlling the collision geometry in Cu+Cu compared to peripheral Au+Au collisions results in higher precision in the suppression measurement, allowing stringent tests of the evolution with increasing system size. An important advance for this run was the implementation of a high p_T (“high tower”) trigger based on the observation of a high energy deposition in a calorimeter tower. This greatly increased the capability of the detector to sample the full RHIC luminosity and to increase the p_T reach of the Cu+Cu measurements.

The evolution of elliptic flow (v_2) with system size is illustrated in Fig. 2 which shows v_2 as a function of p_T for minimum bias collisions for both Au+Au and Cu+Cu using three different measurement methods. The three methods have different sensitivity to correlations unrelated to the reaction plane (non-flow) and to event-by-event fluctuations in v_2 . They agree reasonably well in Au+Au, but diverge strongly in Cu+Cu collisions at high p_T , showing that these effects are relatively larger for the smaller system. The v_2 determined by perhaps the most reliable measure, in which non-flow correlations measured in p+p collisions have been subtracted (AuAu-pp), is significantly smaller in Cu+Cu than in Au+Au. However, more precise p+p reference data are needed to strengthen this conclusion at high p_T . These results have spurred further work on both measurement techniques and the modeling of the underlying geometry using Glauber calculations.

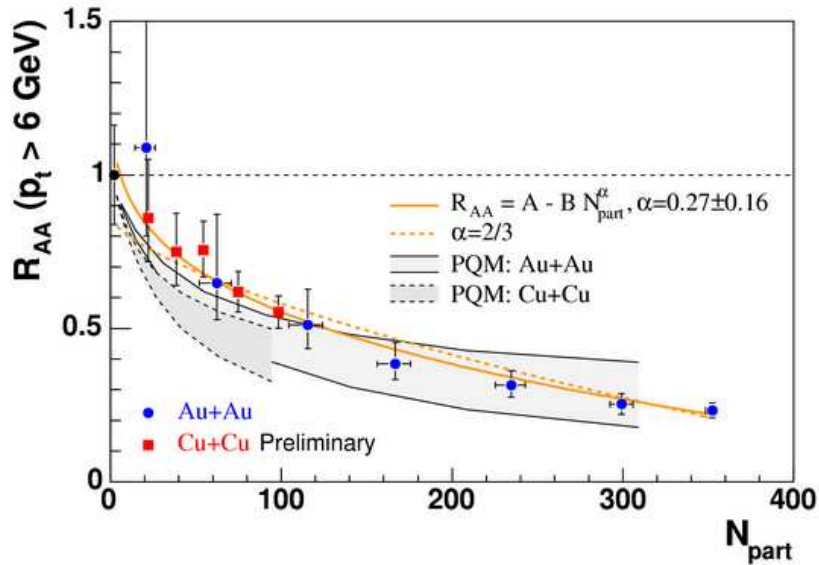
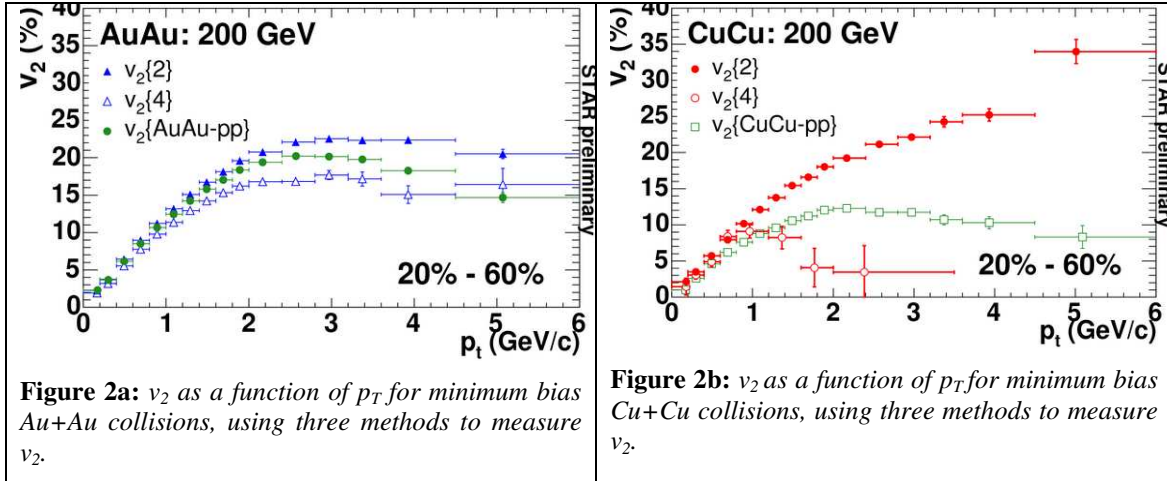
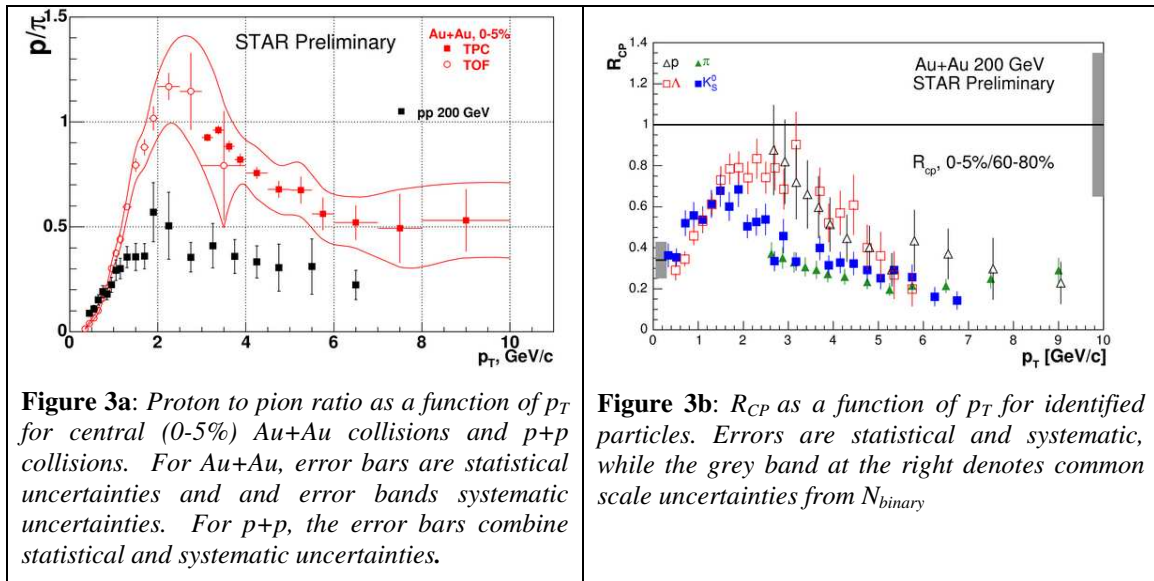


Figure 1: Nuclear modification factor R_{AA} for $p_T > 6 \text{ GeV}/c$ as a function of N_{part} for Cu+Cu and Au+Au. Error bars for Cu+Cu and Au+Au data include statistical and point-to-point systematic uncertainties, which are dominated by uncertainties in the modeling of the collision geometry. Common uncertainties from the p+p reference dataset have been folded into the p+p data point at the left.



Another important advance in Run V was to combine TOF information from a prototype detector for the STAR barrel TOF upgrade with specific ionization (dE/dx) measured in the Time Projection Chamber (TPC) to enable measurement of electrons at intermediate p_T and identification of pions and protons from low p_T (~ 0.5 GeV/c) out to $p_T > \sim 12$ GeV/c. This increased STAR's particle identification capability significantly extending the reach of measurements such as the baryon to meson ratio as a function of p_T .

It was first observed in run 2 that at intermediate p_T ($p_T < \sim 6$ GeV/c) baryons behave differently in heavy ion collisions than mesons. This is shown clearly by Fig. 3a, which shows the ratio of proton to pion spectra in both central Au+Au collisions and in p+p collisions. The large enhancement in Au+Au collisions of the ratio at intermediate



p_T indicates that the dominant source of particle production in this p_T range is not jet fragmentation in vacuum. Utilizing the high statistics obtained in Run 4 and STAR's particle identification capability, the enhancement is observed to be maximal for $p_T \sim 2-3$ GeV/c, beyond which the ratio decreases towards the value observed in p+p collisions.

Whether the ratio in Au+Au reaches that seen in p+p at high p_T is difficult to determine with the present level of statistical and systematic uncertainty.

The enhancement also is evident in the nuclear modification factor R_{CP} , the ratio between central and peripheral Au+Au collisions of N_{binary} -scaled spectra (Fig. 3b). As with v_2 , baryons and mesons are clearly differentiated in the behavior of R_{CP} as a function of p_T . The ϕ and K^* mesons which have masses similar to that of the proton, nevertheless follow the behavior observed for lighter mesons, indicating the observed separation is not related to particle mass. Indications from previous runs that the dependence on hadron species disappears at high p_T were strengthened significantly based on analysis of the run 4 dataset, supporting the applicability of models incorporating parton energy loss for $p_T > \sim 6$ GeV/c.

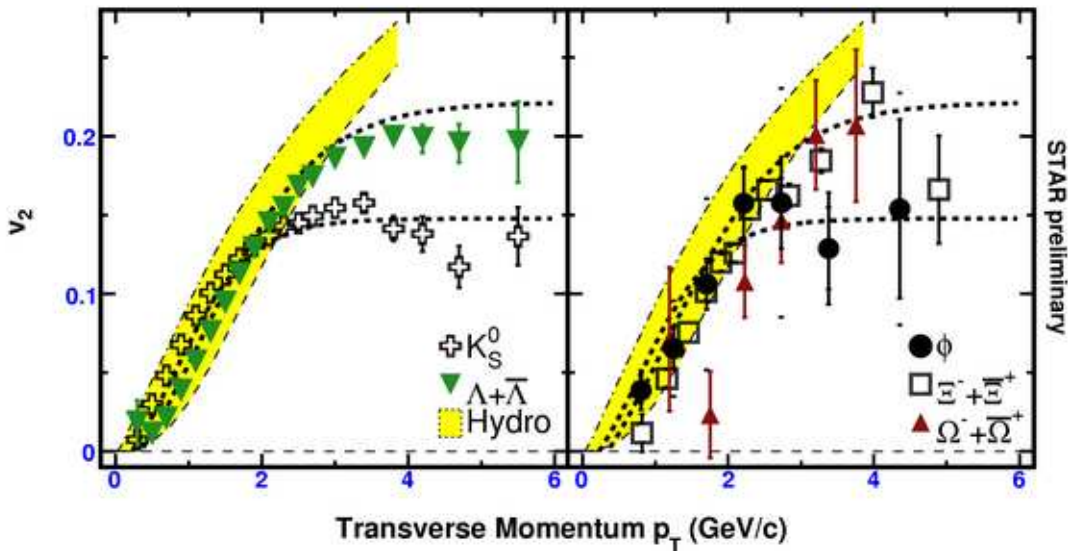


Figure 4: Elliptic azimuthal anisotropy v_2 for identified particles. Dashed lines are indicated to guide the eye. The yellow band denotes the range of hydrodynamic predictions for particles from p to Ω .

The different behavior between baryons and mesons at intermediate p_T also appears in the elliptic azimuthal anisotropy, v_2 . Fig. 4 shows v_2 for various identified hadrons up to the triply-strange Ω baryon for minimum bias collisions. Significant v_2 is seen for all particle species. At low p_T , v_2 is ordered by mass, as expected from hydrodynamic calculations, while at intermediate p_T the ordering is determined by hadron species (meson vs. baryon). To elucidate this behavior, Fig. 5 shows the scaled v_2 , where both v_2 and p_T have been scaled by n , the number of constituent quarks in the hadron (2 for mesons, 3 for baryons). The increased statistical reach of the year 4 Au+Au data allows this scaling to be measured with high precision. At intermediate p_T , v_2 scales well with the number of constituent quarks, lending strong support to the idea that the dominant production mechanism for particles in this range of p_T is coalescence of constituent quarks having a high degree of collectivity. At low p_T , this scaling is clearly violated as noted above. At high p_T more precise results are needed to probe the expected violation of this scaling.

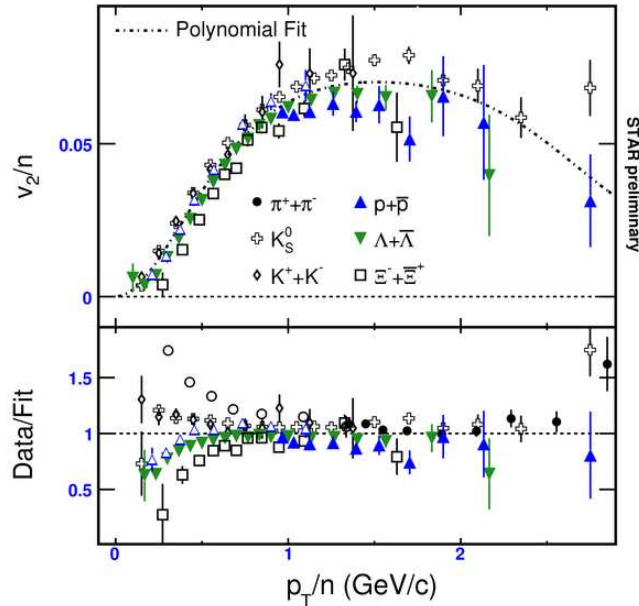


Figure 5: Top: scaled elliptic azimuthal anisotropy v_2/n vs. p_T/n , where n is the number of constituent quarks in a hadron (2 for mesons, 3 for baryons). The line shows a phenomenological fit to the combined data. Bottom: ratio of v_2/n to universal scaling based on the combined phenomenological fit.

Another STAR capability which was dramatically increased in runs 4 and 5 was the ability to measure heavy flavor. In large measure this was due to the commissioning of a large fraction (2π in azimuth, $0 < \eta < 1$) of the barrel electromagnetic calorimeter (BEMC). When combined with information from the main tracking detector (TPC), information on the electromagnetic energy deposited in the BEMC enables the measurement of electrons and photons out to high transverse momentum.

The radiative energy loss of heavy quarks (charm and bottom) to the dense medium created in heavy ion collisions is of prime interest. It is expected to be less than that of light quarks and gluons, due to the c and b quark mass. Therefore, the suppression of mesons containing heavy quarks may be used to test models which incorporate partonic energy loss as well as their dependence on the density of the medium.

Within STAR, heavy flavor can be accessed directly on a statistical basis through combinatoric subtraction of background from the distribution of invariant mass reconstructed from hadronic decay products (e.g. $D^0 \rightarrow K\pi$ at low p_T) or indirectly by measuring the spectrum of “non-photonic” electrons from semi-leptonic decays. The dominant source of electrons observed in the detector is the conversion of photons produced by hadronic decays (e.g. $\pi^0 \rightarrow \gamma\gamma$). Dalitz decays also play a role. These backgrounds can be subtracted using an invariant mass technique: the resulting non-photonic electrons are expected to come predominantly from the decay of mesons containing charm and bottom.

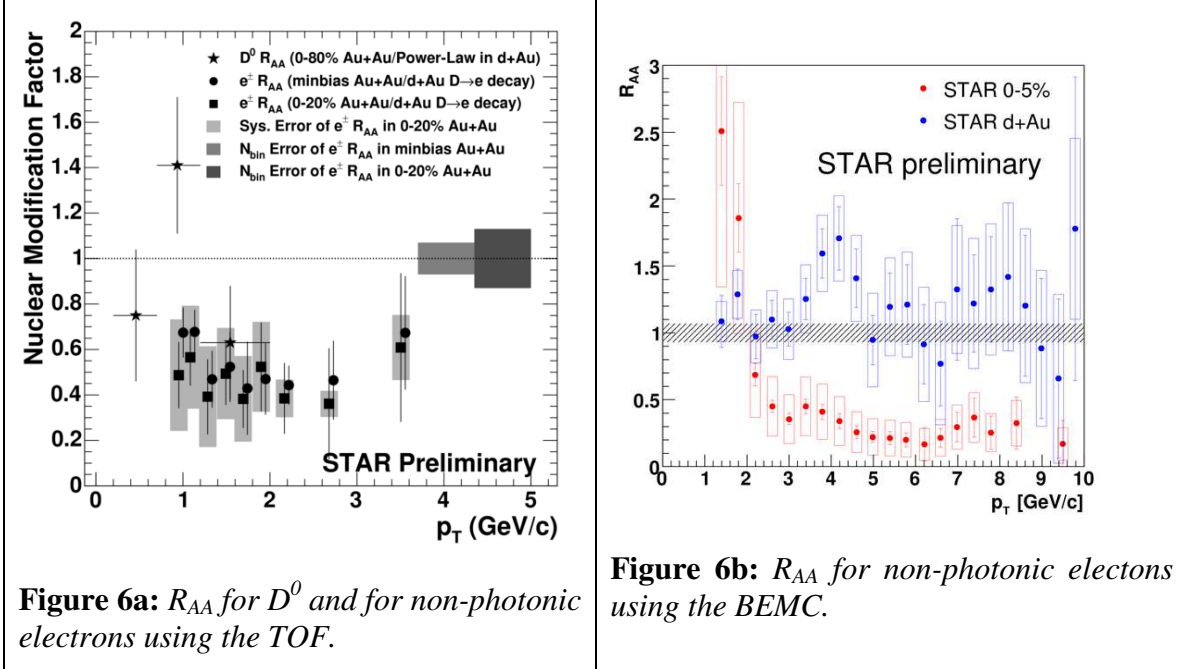


Figure 6a: R_{AA} for D^0 and for non-photonic electrons using the TOF.

Figure 6b: R_{AA} for non-photonic electrons using the BEMC.

Figures 6a and 6b show recent results on the p_T suppression of heavy flavor. The total cross-section of charm production, determined predominantly by the direct measurement of D^0 mesons at low p_T , is found to scale with N_{binary} , as expected for “hard probes” produced in the initial stages of the collision. At higher p_T however, surprisingly, strong suppression similar to that observed for light hadrons is observed out to $p_T \sim 10$ GeV/c. This result differs significantly from the suppression predicted ($R_{AA} \sim 0.5-0.6$) for non-photonic electrons in this p_T range. The suppression can be reproduced assuming radiative energy loss in a medium of extreme density, but only if the contribution from bottom decays is assumed to be negligible. Resolving the true level of suppression for charm and bottom will ultimately depend on measuring their contributions separately. Detector upgrades to accomplish this are being developed.

One means to access the energy loss of a parton in the medium is to tag on a direct photon from a hard parton scattering, and then examine the fragmentation products of the away-side jet. Since the photon exits directly from the collision zone, this can be accomplished by examining the strength of the correlation in azimuth between the photon and fragmentation hadrons from the away-side jet for a given range of p_T . Experimentally, this measurement is complicated by large contributions from π^0 decay photons and the low cross section for $\gamma + \text{jet}$ coincidences in a measurable range of p_T .

Figure 7 shows first results for this measurement from run 4. A photon having $E_T > 10$ GeV/c in the BEMC is tagged and correlated in azimuth with all hadrons having $4 < p_T < E_T^{\text{trigger}}$. For this result, 180M minimum bias events were presented to the trigger, corresponding to a sampled luminosity of $\sim 25 \mu\text{b}^{-1}$. Clear near and away-side peaks are seen as expected from high Q^2 parton-parton scattering. Separation of the contribution of direct and hadronic photons to the azimuthal correlation function is a work in progress.

Ultimately, full exploitation of this technique will require the large increase in luminosity planned for RHIC II.

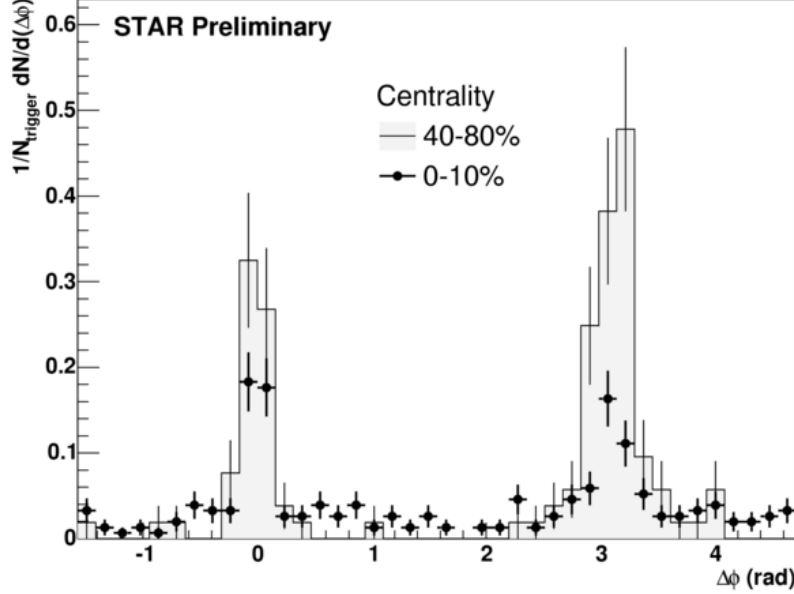


Figure 7: Au+Au collisions at $\sqrt{s_{NN}} = 200$ GeV: per-trigger azimuthal correlation of charged hadrons associated with a trigger photon. The trigger photon has $E_T > 10$ GeV/c, while the associated charged hadrons have $4 < p_T^{assoc} < E_T^{trigger}$

Another source of information is pair-wise correlations in azimuth and pseudorapidity between hadrons. Jet-like correlations have been found to persist to extremely low p_T (below 2 GeV/c), as shown in Fig. 8. Dramatic changes in the shapes of these correlations are seen in the progression from peripheral (lower right) to central (upper left) Au+Au collisions. The near-side peak widens substantially in η (by a factor of 2.3) from peripheral to central collisions, indicating strong coupling between these correlated particles and the longitudinal expansion of the medium. Such measurements are possible because of the large η acceptance of the STAR TPC. In the future, their full interpretation will benefit greatly from the additional particle identification capability provided by the barrel TOF upgrade.

Somewhat higher in transverse momenta, when both the “trigger” hadron and the associated particles are in the intermediate p_T regime, strong modification of the away-side peak shape is seen. Figure 9 shows results for one choice of p_T threshold as a function of centrality. As the collisions become more central, the population of the two-particle correlation at intermediate angles (from ~ 1.5 to 2.5 radians) grows significantly. Various interpretations for the origin of this enhancement have been given including the possibility that energetic particles may exceed the speed of sound in the medium creating a shock front. This study is an area of very active investigation.

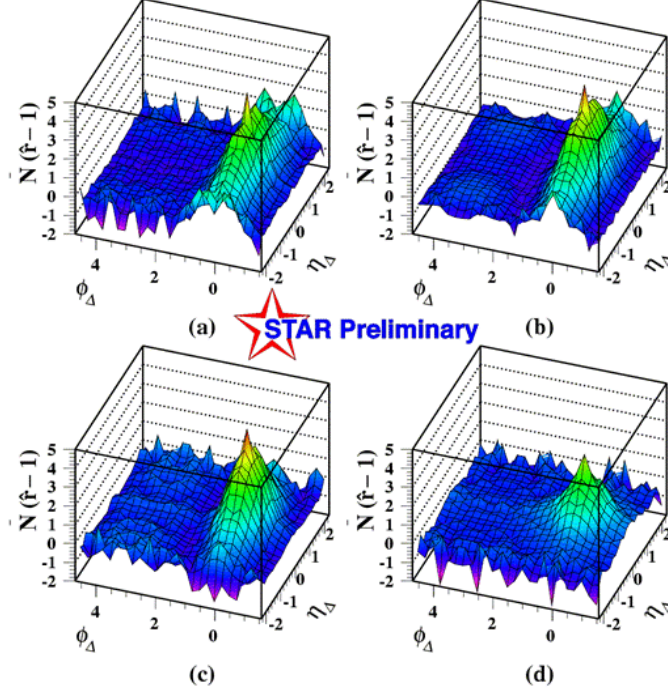


Figure 8: For Au+Au collisions at $\sqrt{s_{NN}} = 200$ GeV: pair-wise correlations in azimuth (ϕ_{Δ}) and pseudorapidity (η_{Δ}) between soft particle pairs with $0.15 < p_T < 2$ GeV/c for (a) central to (d) peripheral collisions. Independent first and second harmonics have been subtracted.

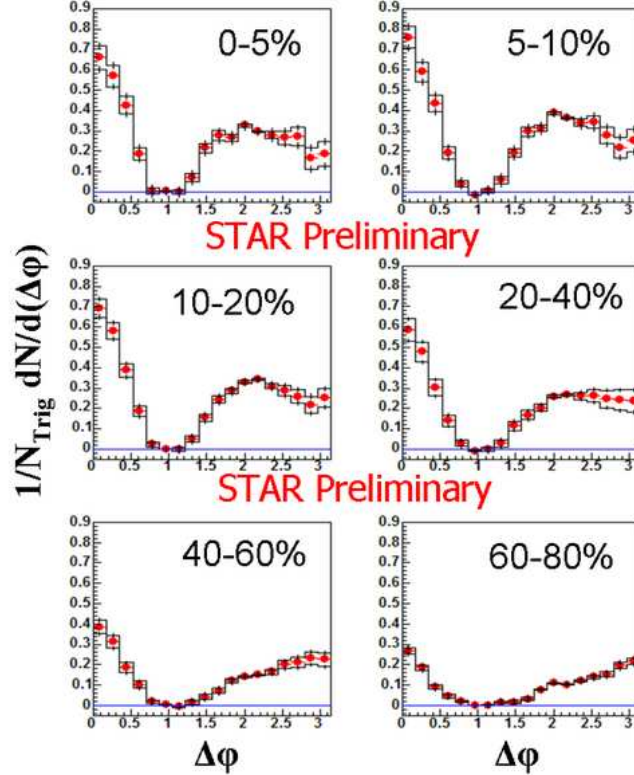


Figure 9: Au+Au collisions at $\sqrt{s_{NN}} = 200$ GeV: per-trigger azimuthal correlations at different centralities with $2.5 < p_T^{trig} < 4.0$ GeV/c, $|\eta^{trig}| < 0.7$, and $1 < p_T^{assoc} < 2.5$ GeV/c, $|\eta^{assoc}| < 1$.

Deeper insight into the origin of this observation may be provided by three-particle correlations which tend to suppress trivial effects e.g. due to momentum conservation. Shown in figure 10 are first results on 3-particle correlations for d+Au reference data and central Au+Au collisions.

One interpretation of the additional population observed in the two-particle correlations at intermediate angles for central collisions is that it is due to conical flow induced by shock waves in the non-viscous medium created in heavy ion collisions. If so, sufficiently strong conical flow would result in an enhancement in the off-diagonal region ($\pi-1$, $\pi+1$ and $\pi+1$, $\pi-1$) in three-particle correlations. No such enhancement is found; instead, the diagonal ridge is extended, as might be expected from radial flow or increased k_T smearing in central Au+Au collisions. This initial study will be carried out with larger Au+Au datasets in the future.

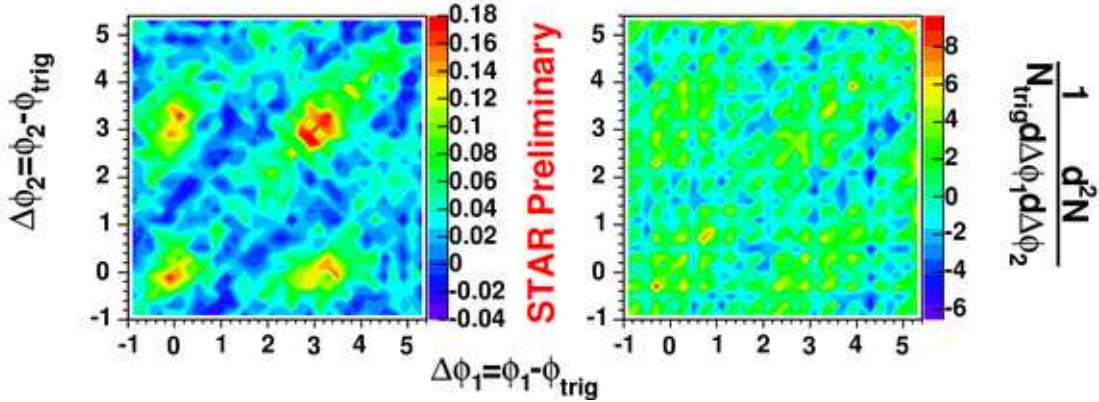


Figure 10: Three-particle correlations in minimum bias d+Au collisions (left) and 10% central Au+Au collisions (right). The p_T ranges are $3 < p_T^{\text{trig}} < 4$ GeV/c and $1 < p_T^{\text{assoc}} < 2$ GeV/c.

The higher statistics available from the run 4 Au+Au data sample have allowed extension of hadronic correlation measurements to the high p_T region in which e.g. the baryon-meson splitting in R_{cp} is no longer apparent. Figure 11 shows two-particle azimuthal correlations in this region. Clear near and away-side peaks are seen. The combinatoric background upon which they sit is greatly reduced, negligible even in central Au+Au collisions for the highest p_T thresholds investigated. The strong modifications in the peak shapes observed for low p_T thresholds are not apparent for these higher p_T thresholds, indicating the correlations observed in this regime result primarily from the fragmentation of di-jets.

The clean identification of correlations generated by di-jets, allows investigation of hadron-triggered “fragmentation functions”, by binning the correlations in $z_T = p_T^{\text{assoc}}/p_T^{\text{trig}}$ and integrating the near- and away-side peaks (Fig. 12). The near-side fragmentation function is unchanged from d+Au collisions to central Au+Au collisions, but the away-side fragmentation function is strongly suppressed, comparable to the level of suppression observed for single-particle inclusive spectra. Di-hadron correlations

incorporate a completely different set of biases (induced by fragmentation and the geometry of the overlap region) than single-particle spectra. Therefore, such measurements place constraints on the density of the medium which are somewhat independent of those derived from the suppression of inclusive spectra. Combining the information from both observations may allow the determination of an upper bound on the density of the medium. This, in combination with a lower bound on the entropy density of the medium, may lead to a lower bound on the number of degrees of freedom of the medium². The precision of di-jet measurements in STAR is currently limited by the precision of reference data from d+Au: additional reference data will greatly improve the reach of this measurement.

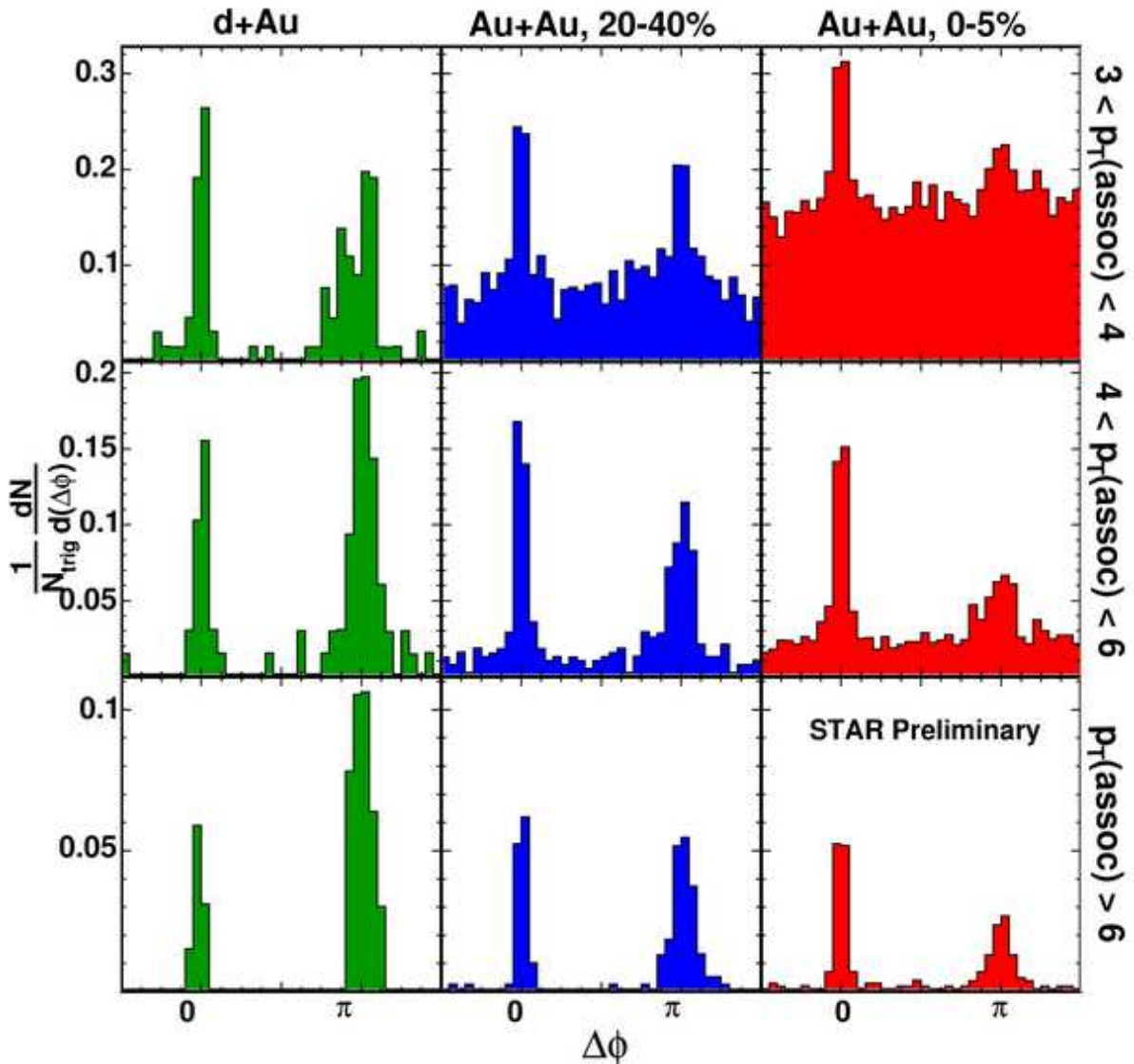


Figure 11: Per-trigger azimuthal correlations between charged hadrons for the systems indicated at $\sqrt{s_{NN}} = 200$ GeV. The “trigger” hadron has $8 < p_T < 15$ GeV/c.

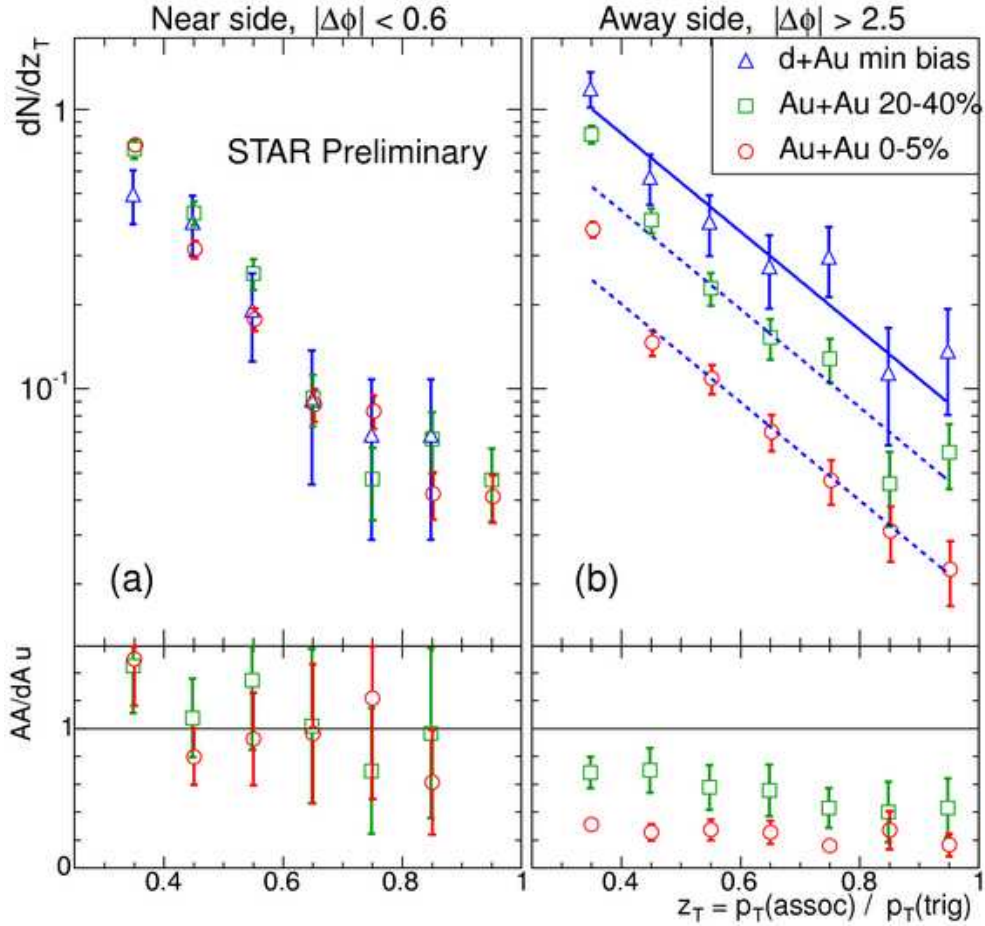


Figure 12: Top: Di-hadron “fragmentation functions” as a function of z_T for minimum bias $d+Au$ collisions and $Au+Au$ collisions at two centralities. The lines are from an exponential fit to the $d+Au$ data, scaled down by a p_T -independent factor to results in $Au+Au$ collisions. Bottom: ratio between results from $Au+Au$ and $d+Au$ collisions.

2. Proposed Beam Use for Run VI (2005-2006)

For Run 6, the STAR Collaboration proposes a suite of complementary spin physics measurements with transverse and longitudinal polarization that will allow a qualitative advance in the worldwide impact of RHIC spin results. Recent spin physics progress in STAR as well as the feasibility and urgency of the measurements proposed for Run VI are detailed in the sections which follow.

Provided the spin physics goals proposed for Run 6 are completed with sufficient remaining time, STAR proposes a short $Au+Au$ run with 1 week of data taking at each of two energies, $\sqrt{s_{NN}} = 19.6$ and 31 GeV.

The primary STAR beam use request during Run 6 is for 30 pb^{-1} of sampled/recorded p+p collisions at $\sqrt{s} = 200 \text{ GeV}$ with 50% or greater polarization in each beam. After accounting for losses due to detector up-time, data acquisition live time, etc., comparable to those during Run 5, this will require C-AD to deliver 90 pb^{-1} . If one assumes the average of the projected minimum and projected maximum accelerator performance estimated by C-AD, this will require ~ 20 weeks of polarized proton physics running during Run 6.

STAR proposes to devote 20 pb^{-1} of recorded luminosity for longitudinal spin running. This will represent an order-of-magnitude increase in the integrated longitudinal figure-of-merit, P^4L , compared to that obtained in Run 5. This will lead to significant improvements in the precision of the STAR measurements of the gluon polarization within the nucleon using inclusive jets and π^0 's. While the Run 5 results will allow us to distinguish between various extreme (and disfavored) gluon polarization scenarios, the new results that will come from the proposed Run 6 will distinguish – for the first time – amongst the various gluon polarization scenarios that are favored in current global analyses. Moreover, Run 6 measurements will permit the first studies of rare channels not measured thus far at RHIC that are essential in order to determine not just the overall magnitude of Δg , but the x dependence of the gluon polarization as well.

STAR proposes to devote 10 pb^{-1} of recorded luminosity for transverse spin running. This will provide well over an order-of-magnitude increase in the integrated transverse figure-of-merit, P^2L , compared to that obtained in Runs 2, 3 and 5 combined. During the previous runs, STAR has measured large single-spin analyzing powers, A_N , for inclusive π^0 production at large x_F . These have been explained using a number of different physical models, including the Sivers and Collins effects. The Sivers effect associates the single-spin asymmetries with parton k_T and orbital motion in the incident proton, whereas the Collins effect attributes the effects to quark transversity combined with the Collins fragmentation function. The increased figure-of-merit of the Run 6 data will permit qualitatively new measurements to discriminate between these different physical pictures and to explore whether effects that play a role at large rapidity may also be acting in a more subtle manner in the mid-rapidity region at RHIC.

During the spin running, some time will probably be spent at beam momenta well above $100 \text{ GeV}/c$ to evaluate the effects of the realignment of RHIC. STAR supports a few days for such studies, as they are important for future $\sqrt{s} = 500 \text{ GeV}$ measurements. STAR also encourages the polarized jet target to be operational during most of the run. This will permit a validation of the stability of the p+C CNI polarimeter absolute calibrations.

The next subsection describes several significant improvements to the STAR detector and trigger system since Run 5 that will play crucial roles in the polarized proton measurements during Run 6. For certain measurements, these improvements constitute enabling technologies that make the measurements possible for the first time. Meanwhile, all of these improvements will serve to increase STAR's data taking efficiency, leading to much better statistical reach for several measurements than would be implied by the increased figures-of-merit alone.

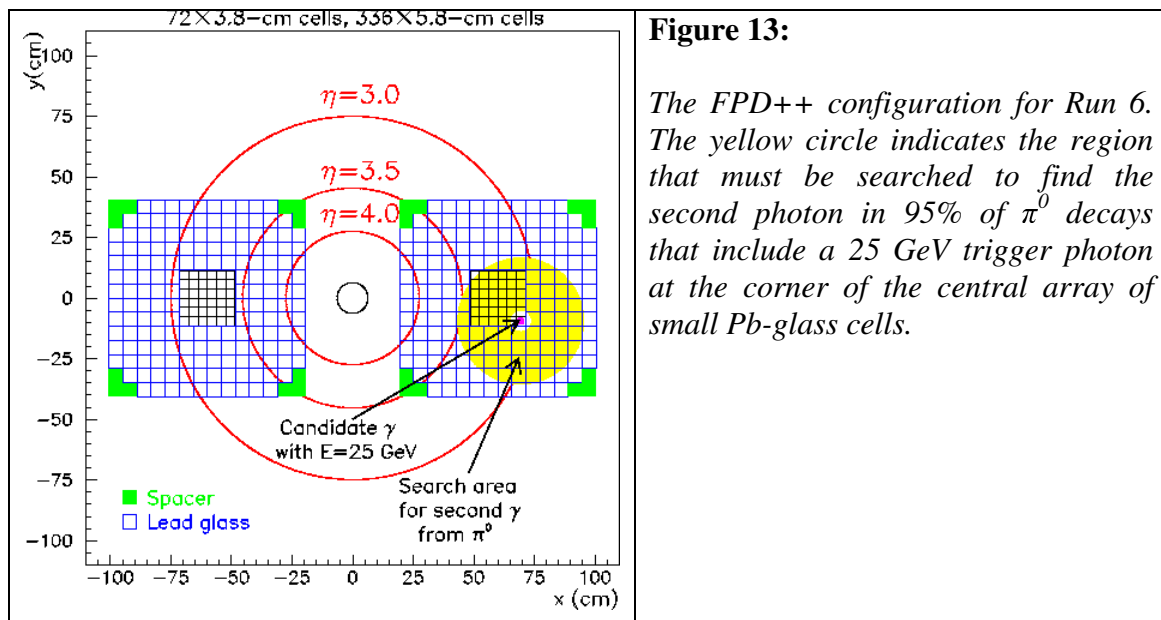
2.1 Modifications to the STAR Detector Configuration for Run VI

Over and above the anticipated order of magnitude improvement in integrated figure of merit for polarization measurements that would come from the proposed long p+p run, a number of hardware and software improvements to STAR will substantially enhance STAR's efficiency in attaining the scientific goals outlined in this request. The improvements that are discussed below include: (1) completion of the readout electronics for the Barrel ElectroMagnetic Calorimeter (BEMC) and inclusion of the full BEMC coverage in the STAR L0 trigger; (2) reconfiguration of the Pb-glass Cerenkov counters forming the west Forward Pion Detector (FPD) to provide enhanced acceptance (FPD++) for forward photons and π^0 's on one side (west) of STAR; (3) introduction of extensive iron shielding in the RHIC tunnels leading to STAR on both east and west sides, to reduce the hadronic background seen by the EMC's; (4) use of the STAR level 2 trigger to enhance efficiency and selectivity of triggers for di-jet events and for direct photons and π^0 's in the $p_T = 5-10$ GeV/c range.

One of the major physics goals highlighted herein for the requested 10 pb^{-1} of sampled luminosity with transverse (vertical) beam spin orientations is the measurement of single-spin asymmetries for not-quite-back-to-back di-jets, an effect with leading-twist sensitivity to potential Sivers functions in the proton (correlations between proton transverse spin and parton transverse motion preferences). Jet production is an abundant process, and STAR's acquisition of jet events is limited by DAQ rate capabilities rather than by luminosity. Nonetheless, the acquisition rate of di-jet events should be enhanced by a factor of 5 or more by the improvements under way. Of ~ 40 Hz of jet (L0) triggers collected by STAR during the 2005 run, only ~ 2 Hz contained reconstructable di-jets within the fiducial pseudorapidity range ($0.2 < \eta < 0.8$) limited by the then-commissioned west half of the BEMC. The doubling of the BEMC fiducial range will automatically improve the di-jet fraction. We anticipate devoting ~ 10 Hz of L0 trigger bandwidth during transverse spin running to a BEMC-based jet patch trigger (summed E_T over $\Delta\eta \times \Delta\phi = 1.0 \times 1.0$ patches) with a threshold set sufficiently high (4-5 GeV) that no prescaling of the L0 rate is required. That sample should then contain $\sim 30\%$ (up from 15% in 2005) di-jet events. Another ~ 10 Hz sample, corresponding to jet patch triggers at lower threshold, was heavily prescaled in 2005, leading to a random sample of events with di-jets in only $\sim 6\%$. In 2006 we will instead use a L2 trigger algorithm designed to select events with substantial EMC energy deposition also at opposite ϕ from the L0 trigger region. The combination of doubled BEMC coverage and L2 trigger selectivity should yield at least a $\sim 50\%$ enrichment of the lower-threshold events in di-jets.

Additional contributions to the di-jet yield will come from high-tower triggers and from endcap EMC (EEMC) triggers. Ongoing improvements to STAR tracking software in the $|\eta| > 1.4$ region will enhance reconstruction efficiency for di-jets from EEMC triggers. The enrichment of these triggers in di-jet events will be further improved by the shielding additions. In 2005, typically 1/3-1/2 of EEMC jet patch triggers were caused by high-energy hadrons from upstream background sources in accidental coincidence with a minimum-bias collision at STAR; that fraction is expected to be drastically reduced by

the shielding presently being installed in the RHIC tunnels. The shielding will hopefully improve STAR's efficiency in using delivered luminosity, as less time should be needed for careful beam tuning to reach minimally acceptable backgrounds at STAR near the beginning of each fill. The shielding is also critical to the di-jet measurement in a more subtle way. The upstream background observed in STAR's EMC's during 2005 had a highly anisotropic azimuthal distribution, dominated by yield near "10:30", looking toward the IR from the west side of STAR. (That distribution is qualitatively consistent with expectations based on shielding from the tunnel floor and from the iron in the sleeve of the D0 magnet to the east of STAR.) One such background hadron showering in an EMC in accidental coincidence with a di-jet event can significantly distort the crucial measurement of $\delta\phi$ between the two jet axes. If the rate of background differs from beam bunch to beam bunch, depending on the beam halo, a significant instrumental Sivvers asymmetry could be produced. The shielding being installed between the DX and D0 magnets to the east and west of STAR is therefore viewed as crucial as well for suppressing such systematic errors in the di-jet asymmetry measurement.



Additional major physics goals of the transverse spin running at STAR are measurements of single-spin asymmetries for jet-like events and direct photon production at high rapidity in order to separate the effects of parton orbital motion (Sivers effect) from those of transversity (Collins effect). For this program, the reconfiguration of the west FPD into the FPD++ is crucial.

The FPD++ is an intermediate step toward the full STAR Forward Meson Spectrometer (FMS), which will be in place for Run 7. The FPD++ consists of two calorimeters as shown in Fig. 13, symmetrically positioned left and right of the beam, 7.5 m west of the STAR interaction point. Each calorimeter includes a 6x6 array of 3.8-cm square Pb-glass cells from the disassembled west FPD, surrounded by 5.8-cm square Pb-glass cells to provide nine times the total area of the north and south FPD modules. The increased acceptance will permit a detailed (x_F , p_T) mapping of the transverse single-spin analyzing

powers for large rapidity inclusive π^0 production. More importantly, the calorimeters are sufficiently large to allow efficient isolation cuts, as indicated in Fig. 13. These are essential to identify direct photon production amidst the far more intense flux of energetic hadrons. The FPD++ calorimeters are also large enough to span the jet cone centered on a leading hadron within the small central array, which will enable measurements of spin effects for jet-like events.

The ongoing improvements have significant impact as well on attaining STAR's science goals from the requested 20 pb^{-1} of sampled luminosity with longitudinal beam polarization, where the largest share of the combined trigger bandwidth for high tower and jet patch EMC triggers will be given to the high tower component. A major focus is on acquisition of a sufficient sample of direct photons to allow a first measurement of A_{LL} for this channel, while perfecting analysis algorithms for photon reconstruction and discrimination from π^0 's in preparation for the heavy emphasis on photon production anticipated for subsequent, higher-luminosity p+p runs. Clearly, inclusion of a fully commissioned BEMC and a reconfigured FPD++ in STAR's L0 trigger enhances our (high-tower) trigger efficiency and kinematic acceptance for photon events. In order to reach our eventual statistical precision goal for direct photon and γ +jet events in STAR in the $\sim 90 \text{ pb}^{-1}$ of sampled luminosity anticipated for the coming years, it will be important to include photons down to $p_T \approx 5 \text{ GeV}/c$. Efficient triggering down to these momenta, taking into account shower-sharing among EMC towers and present STAR DAQ rate capabilities, will benefit significantly from L2 trigger software under development for the 2006 run. We will be able to run L0 high-tower trigger thresholds at $p_T \approx 2.5 \text{ GeV}/c$ by further L2 filtering to accept only those L0 triggers for which a cluster of adjacent towers including the trigger tower contains a summed energy deposition equivalent at least to $p_T \approx 5 \text{ GeV}/c$. The L2 software should enhance photon trigger selectivity near threshold by roughly 50%, and should furthermore improve π^0 trigger/reconstruction efficiency near threshold by a factor of 2 or more. The latter improvement comes about because the L0 high-tower trigger alone strongly favors π^0 's that decay to two photons with strongly asymmetric energy sharing, while our reconstruction algorithms and shower-maximum detectors favor symmetric energy sharing. Photon and π^0 reconstruction in the east half of the BEMC will be available for the first time in 2006, thanks to the newly installed readout electronics for the shower-maximum and preshower detectors in that half of the BEMC. Finally, the enhanced acceptance provided by completion of the BEMC readout and by the FPD++ reconfiguration (and in the future, the even larger FMS) are critical to STAR's anticipated emphasis in future years on constraining gluon polarization as a function of Bjorken x via coincidence measurements, which will be essential to determine the shape of the polarized gluon distribution function as a function of x .

2.2 Proposed gluon polarization measurements with longitudinal polarization

The STAR measurement program to determine the polarization of gluons in a polarized proton is envisioned to proceed in three stages. The first, already under way, will provide an initial survey of the scale of Δg via study of abundant inclusive reaction channels – jet

and π^0 production – in polarized pp collisions at $\sqrt{s}=200$ GeV. The second, fueled by increases in luminosity and beam polarization, will explore rarer channels such as direct photon production, that offer complementary sensitivity to Δg , with emphasis on γ -jet coincidence studies that permit a direct experimental map of the dependence of Δg on Bjorken x . The third stage will extend the measurements to 500 GeV to probe x -values between 0.01 and 0.05 – where a large fraction of the integral gluon polarization is anticipated to reside – and provide some information on the Q^2 -dependence of the gluon polarization. The beam time requested herein for 2006 – 20 pb^{-1} of sampled luminosity at STAR with longitudinal beam polarization – will allow a transition from the first to the second stage of this program. It will allow measurements of the two-spin helicity

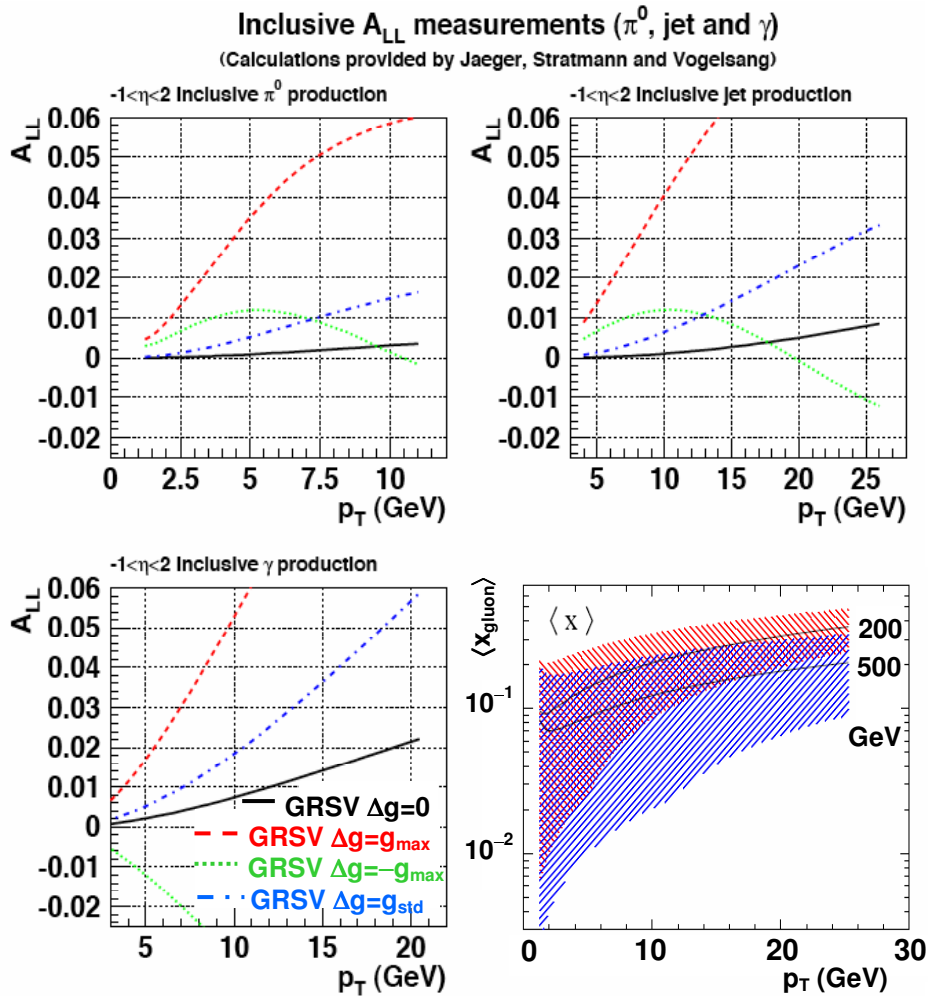


Figure 14. NLO pQCD predictions for inclusive jet, π^0 and direct photon production. The upper two frames and the lower left frame show A_{LL} within the STAR calorimeter acceptance as a function of p_T under different assumptions for the underlying polarized gluon distribution: no gluon polarization (solid black); standard GRSV³ fit to polarized deep inelastic scattering database (dot-dashed blue); gluon distributions evolved from +100% (dashed red) or -100% (dotted green) polarization at an initial low Q^2 scale. The lower right frame shows the gluon x -ranges contributing to inclusive π^0 production in $p+p$ collisions at $\sqrt{s} = 200$ and 500 GeV, with solid curves indicating the mean contributing x -values, and the shaded bands indicating the rms spread of contributing x -values.

asymmetry A_{LL} for inclusive jet and π^0 production with sufficient statistical and p_T reach to provide important constraints on models and parameterizations of $\Delta g(x)$. It will provide a large sample of di-jet coincidences that will constrain the x -values and contributing partonic subprocesses better than inclusive jet measurements. It will furthermore provide a first statistically meaningful sample of γ -jet coincidence events to launch the serious analysis of that crucial channel. Acquisition of sufficient γ -jet statistics to reach our goal of determining $x\Delta g(x)$ to $\sim\pm 0.1$ in each of several $\ln(x)$ -bins will require $\sim 90 \text{ pb}^{-1}$ of sampled cumulative luminosity at an average beam polarization $\sim 65\%$, and thus will require at least one additional long polarized pp run at 200 GeV in the coming years of RHIC operation.

Very encouraging indications for the theoretical interpretability of RHIC spin measurements are provided by the consistency of absolute cross sections already measured by PHENIX⁴ and STAR⁵ for inclusive π^0 and photon production in pp collisions with next-leading-order (NLO) pQCD calculations for $p_T > \sim 2 \text{ GeV}/c$. Nonetheless, comparisons of Δg information extracted from measurements of various reaction channels will be critical to provide convincing evidence that these hadronic probes also yield cleanly interpretable constraints on nucleon spin structure. A more detailed appreciation for the complementarity of the various channels STAR will emphasize is given by Fig. 14, which shows NLO pQCD predictions for inclusive π^0 , jet and photon production. Constraints on Δg from the first two of these channels are strongly affected by the important contributions from gluon-gluon scattering at moderate p_T , which depend on the *square* of the gluon polarization, in contrast to the linear dependence for quark-gluon scattering, and the independence for quark-quark contributions. As a result, π^0 and jet measurements must be extended to high p_T in order to resolve an ambiguity about the sign of gluon polarization. The inclusive direct photon production is dominated by a single partonic channel, $qg \rightarrow q\gamma$, with A_{LL} providing linear, and hence less ambiguous, sensitivity to Δg , albeit in a channel of substantially lower yield. As illustrated by the lower right frame of Fig. 14, all of these inclusive channels provide only a modest correlation between p_T and the x -value of the contributing gluons, and hence limited experimental constraints on the *shape* of $\Delta g(x)$. In contrast, γ -jet⁶ or forward π^0 -hadron⁷ coincidences can determine the x -value of the contributing gluon on an event-by-event basis to a typical precision $\sim\pm 0.02$, providing direct experimental sensitivity to the shape of $\Delta g(x)$.

The proposed 2006 pp run will allow a qualitative advance in the worldwide impact of RHIC spin results. Under conservative assumptions regarding luminosity (taking the mid-point of C-AD projections) and beam polarization (50%, which should be exceeded if the new cold-bore AGS snake can be fully utilized), the proposed run would represent an order of magnitude improvement in the figure of merit ($P^4\mathbf{L}$) for A_{LL} measurements. The completion of STAR's barrel electromagnetic calorimeter (BEMC) readout electronics, implementation of intelligent Level 2 software for EMC-based triggers, and installation of shielding to reduce beam backgrounds that highly contaminated endcap EMC triggers in 2005, will combine to provide additional factors of ~ 2 -5 improvement for particular channels. We thus anticipate improving statistical uncertainties typically by factors of 3

or more, which will in turn permit more penetrating studies of potential systematic uncertainties.

The physics impact can be illustrated in Fig. 15 by projections for the channel that benefits *least* from the improvements. This is inclusive jet production, where acquisition rates are already limited by STAR rate capabilities rather than by luminosity. The

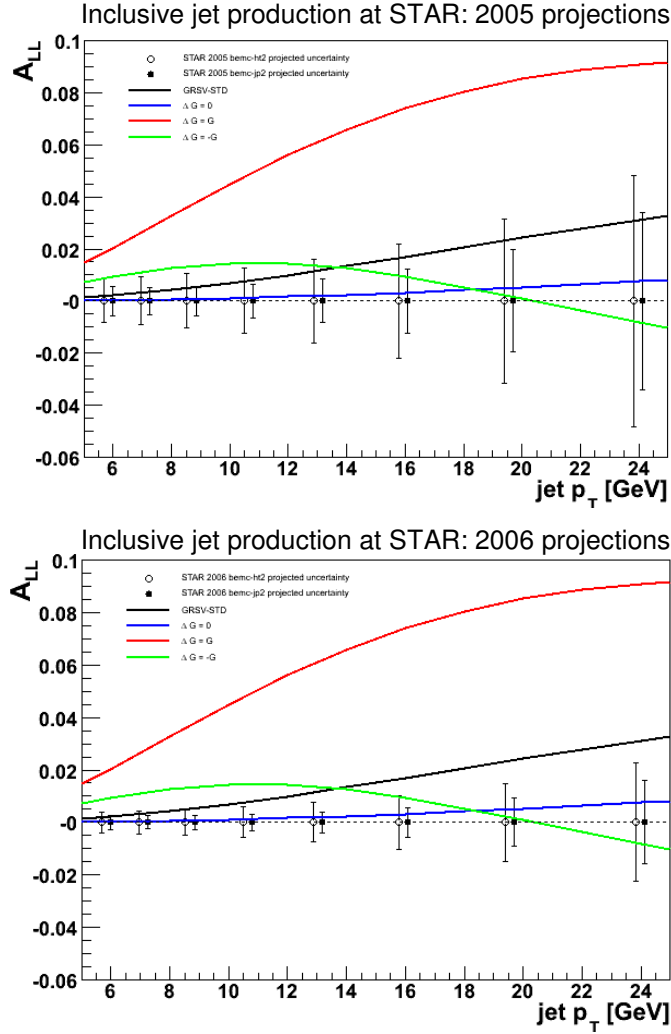


Figure 15. Projected statistical precision for the double-longitudinal spin asymmetry for inclusive jet production from the 2005 (upper frame) and 2006 (lower) runs, for high-tower (*ht2*, open symbols) and jet-patch triggers (*jp2*, closed symbols), in comparison to theoretical predictions made with the same gluon polarization models as in Fig. 14. The 2005 projections correspond to event sample sizes actually collected, on which data analysis has begun. The 2006 projections are based on an assumed integrated luminosity of 20 pb^{-1} , 50% beam polarization and a similar trigger mix and acquisition dead time to the 2005 values. With the increased jet patch trigger thresholds anticipated and an increase to 60% polarization, the error bars for $p_T > 10 \text{ GeV}$ would shrink by another factor of 2.

projections shown in the figure assume we will run with the same jet trigger rates as we did in 2005, and thus benefit only from the increased length of the run, the slight assumed

improvement in beam polarization and the increase in mean number of jets found per triggered event that will accompany BEMC completion. The resulting conservative factor of 2 reduction in error bars would take us from a situation in 2005 where our results (when they become available) can distinguish between extreme and currently disfavored models of gluon polarization, while still leaving considerable ambiguity about the sign of Δg , to a situation where we can distinguish among currently preferred models and between the two signs. In fact, the luminosity increase will force us to raise thresholds to maintain the same trigger rate, so the error bars will improve less than indicated in Fig. 15 for $p_T < 10$ GeV, but by a considerably larger factor at high p_T , improving the overall discriminating power of the results. Indeed, if the beam polarization can be raised to 60% by successful commissioning of the AGS cold-bore snake by the second half of the 2006 run (after our proposed transverse spin running at STAR), then the attainable error bars for jets of $p_T > 10$ GeV would be reduced from those in Fig. 15 by an additional factor of 2, leading to a world-class constraint on Δg .

The two sets of points shown in each frame of Fig. 15 correspond to two different triggers used for our jet data, requiring a high energy deposition in either a single EMC tower (high-tower, “ht2”) or over an EMC patch of size $\Delta\eta \times \Delta\phi = 1 \times 1$ (jet patch, “jp2”). These triggers select largely non-overlapping jet samples with substantially different trigger biases. The jp2 trigger is the most efficient and least biased for jets, but the ht2 trigger is crucial for acquiring photon and π^0 data. We analyze the two samples independently to permit comparative studies of jet trigger bias, but then can combine the results if we find the differences to be small and understood. The error bars from the combined sets would be considerably smaller than those shown in Fig. 15 for jp2 alone. These inclusive jet samples would be further supplemented by a large di-jet sample, taking advantage of the acceptance and L2 trigger improvements noted earlier in this proposal.

In addition to providing real discriminating power for the abundant channels, the proposed 2006 run would yield samples of roughly 250,000 direct photons with $p_T \geq 4$ GeV/c and several tens of thousand γ -jet coincidence events arising from parton collisions involving highly polarized quarks at $x_{quark} > 0.1$, integrated over the acceptance of STAR’s EMC’s. These samples (supplemented by those from the proposed 10 pb^{-1} of transverse spin running) will be critical for the development of photon reconstruction and γ/π^0 discrimination algorithms in the actual detector configuration. While they will not yet yield Δg discriminating power competitive with the inclusive jet results, they should permit the first publication of direct photon A_{LL} results from STAR and allow us to be ready for the prompt analysis and exploitation of γ -jet results from subsequent runs taken with higher luminosity, higher beam polarization and a significantly larger fraction of the trigger bandwidth devoted to this channel. The promise of the full anticipated 200 and 500 GeV γ -jet data sets to constrain $\Delta g(x)$ is indicated by a simplified LO analysis of simulations in Fig. 16.

In addition to the direct photons and γ +jet coincidences that will be detected with the BEMC and EEMC during Run 6, the FPD++ will observe approximately 200,000 direct photons with $p_T \geq 2$ GeV/c and $\eta \sim 3.25$. These direct photons will arise primarily from

quark-gluon Compton backscattering, for which the partonic analyzing power \hat{a}_{LL} approaches unity. Approximately 10% of these events will involve coincident hadrons detected near mid-rapidity. The coincidence requirement will preferentially select events with a large- x quark scattering off a gluon with $x_g \sim 0.01$. These events will provide an alternative look at the low- x gluon polarization. They will also be augmented in Run 7 when the full FMS will be installed.

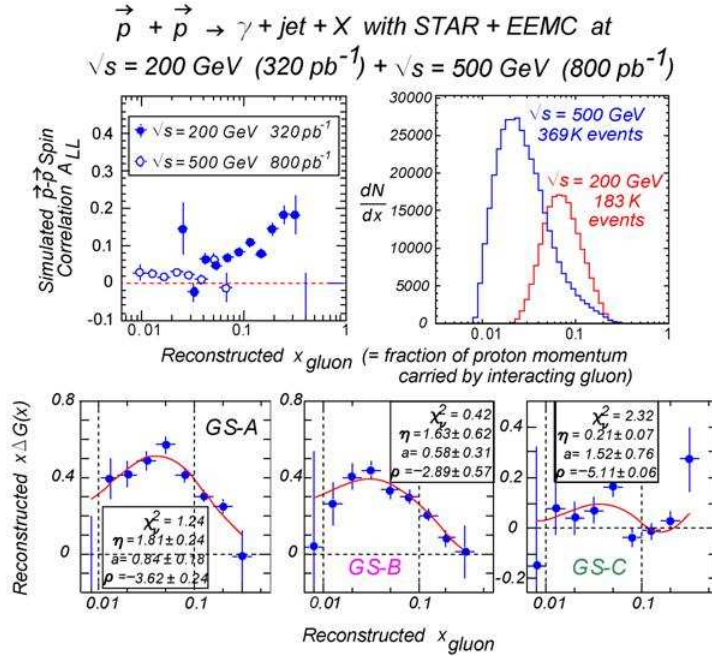


Figure 16. Illustration of $\Delta g(x)$ sensitivities achievable at STAR via A_{LL} simulations for γ -jet coincidences at $\sqrt{s}=200$ and 500 GeV. Upper panels show the distribution of events and projected pp A_{LL} values for one particular parameterization (set A in ⁸) of $\Delta g(x)$, vs. x_{gluon} values reconstructed event-by-event from the coincidence kinematics, under the simplifying assumption of a collinear quark-gluon collision. The lower panels show gluon helicity preferences reconstructed from a LO analysis for three different input gluon distributions [8], plus fits allowing comparison of extracted and input gluon polarizations. The net gluon contribution to the proton spin is given by the area under the $x\Delta g(x)$ curve from $x=0$ to 1. With ~ 90 and $\sim 300 \text{ pb}^{-1}$ sampled, respectively, at 200 and 500 GeV, the very conservative cuts used in this analysis can be relaxed to achieve statistical uncertainties a factor ~ 2 larger than those shown, after γ reconstruction efficiencies and subtraction of residual π^0 background are taken into account.

2.3 Recent Results and Status

2.3.1 Inclusive jet cross sections and asymmetries

STAR acquired inclusive jet samples with limited statistics and predominantly high-tower triggers during the short 2003 and 2004 pp runs. The analysis of these data has been invaluable in the development of algorithms for reconstructing jets, handling EMC hardware problems and calibrations, and assessing and minimizing systematic uncertainties arising from a number of subtle effects: *e.g.*, particles from beam-gas background collisions; trigger bias; and migration of events among p_T bins due to coarse

jet energy resolution and lost energy contributions associated with neutral hadrons or acceptance gaps. These developments now position STAR to make prompt analyses of the far larger jet data samples from the 2005 and 2006 runs. Furthermore, these developments have guided a number of hardware improvements to increase the efficiency of jet data-taking, especially the addition of shielding against beam background, the implementation of more selective jet triggers and better online monitoring of EMC status and performance.

STAR has recently⁹ released preliminary results on double longitudinal spin asymmetries A_{LL} and differential cross sections as a function of p_T for inclusive jet production in proton-proton collisions at $\sqrt{s} = 200$ GeV from data collected in 2003 and 2004. The analyzed data represent an integrated luminosity of ≈ 0.4 pb⁻¹ with average proton beam polarizations of $\approx 30\%$ (2003) and $\approx 40\%$ (2004). Jets are reconstructed in STAR using a midpoint-cone algorithm - with a cone half-angle of 0.4 - to cluster charged tracks from the TPC and electromagnetic energy deposits from the EMC's. The analysis to date has concentrated on high-tower and minimum bias triggers, and on jets with thrust axes within the fiducial pseudorapidity region $0.2 < \eta < 0.8$ defined by the commissioned west half of the BEMC available for the 2003 and 2004 runs. Additional cuts restricted the vertex location for accepted events (to within ± 60 cm of the center of STAR) and the ratio of electromagnetic to full jet energy (to minimize beam background contamination), while also imposing a uniform E_T threshold for all BEMC towers. After cuts, the reconstructed sample contains $\approx 300K$ jets with $p_T \geq 5$ GeV (distributed as shown in Fig. 17), with roughly equal contributions from 2003 and 2004.

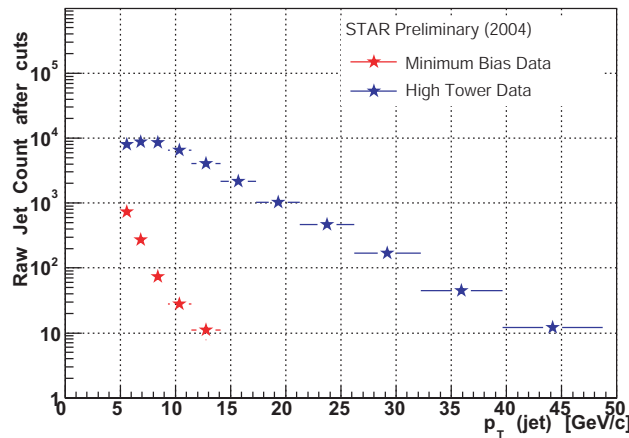


Figure 17. Raw jet yield from 2004 data after applied cuts.

The preliminary A_{LL} results are shown in Fig. 18 with statistical uncertainties only. These error bars are still considerably larger than the estimated cumulative systematic uncertainty of $\approx \pm 0.01$, attributed to uncertainties in the relative luminosity measurements for different beam spin orientations, the trigger bias (high-tower triggers strongly favor quark over gluon jets), possible contributions from residual non-longitudinal beam spin components, the contamination from beam background, and the measurement of the beam polarization (taken here to have a $\pm 25\%$ scale uncertainty). Bunch-to-bunch and fill-to-fill systematic uncertainties were found negligible from analyses with randomized

spin patterns and other cross-checks, such as the analysis of parity-violating asymmetries. Both the STAR and RHIC uncertainties are expected to improve as the program progresses. As is clear from Fig. 18, the present results for A_{LL} do not yet distinguish among the different scenarios for gluon polarization in the proton that are consistent with deep-inelastic scattering data. As suggested in Fig. 15, the 2005 data are expected to conclusively prove or disprove the most extreme scenarios. But adequate understanding of gluon polarization in the nucleon requires far more longitudinal-spin data collection.

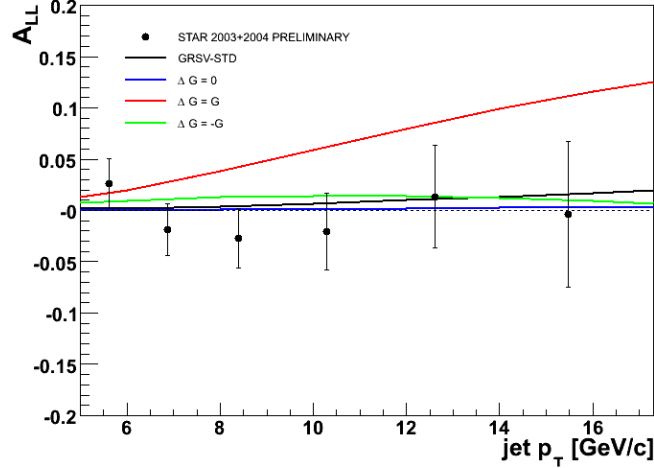


Figure 18. STAR preliminary 2003+4 results for double longitudinal spin asymmetry A_{LL} versus jet p_T in $\bar{p} + \bar{p} \rightarrow jet + X$, compared with NLO p QCD calculations from Fig. 14.

Extraction of absolute jet production cross sections is more challenging than the measurement of spin asymmetries, as it requires a full understanding of absolute trigger efficiencies. In the short term, STAR's inclusive jet cross section measurement serves as a baseline for the interpretation of A_{LL} , cross-checking our understanding of the contributing processes and backgrounds within each analyzed p_T bin. In the longer term, high statistics measurements of inclusive jet and di-jet yields could significantly constrain large- x parton distribution functions (pdf's), in the same way that high- p_T jet yields from the Tevatron drive the large- x region of the CTEQ 6 pdf sets. Given the small sampled luminosity ($\sim 0.16 \text{ pb}^{-1}$ considered so far, from the 2004 run only) and partially commissioned EMC and jet triggers, the preliminary results shown in Fig. 19 serve as a 'proof of principle' measurement.

Analysis of full PYTHIA plus GEANT3 simulations of jet production, triggering, reconstruction and resolution within STAR was a critical component in extracting absolute cross sections. The simulations reveal an overall p_T resolution $\sigma \sim 25\%$ for jets with $10 < p_T < 50 \text{ GeV}/c$, and allow us to determine the p_T distribution of generated parents ("PYTHIA jets") for jets reconstructed within a given p_T bin. Bins were chosen $\sim 1\sigma$ wide in order to maintain diagonal parentage coefficients (fraction of reconstructed jets with generated parents from the same bin) close to 40%. The simulation could then be used to derive a bin-by-bin correction factor convoluting the effects of trigger efficiency, single jet finding efficiency, and bin smearing effects from the $\sim 25\%$ resolution. For the minimum-bias data, where the (BBC-based) trigger is $\sim 90\%$ efficient,

these correction factors remain within 10% of unity. However, for the high-tower trigger, they change from ~ 100 (i.e., 1% efficiency) to ~ 1 in p_T bins from 5 to 50 GeV/c.

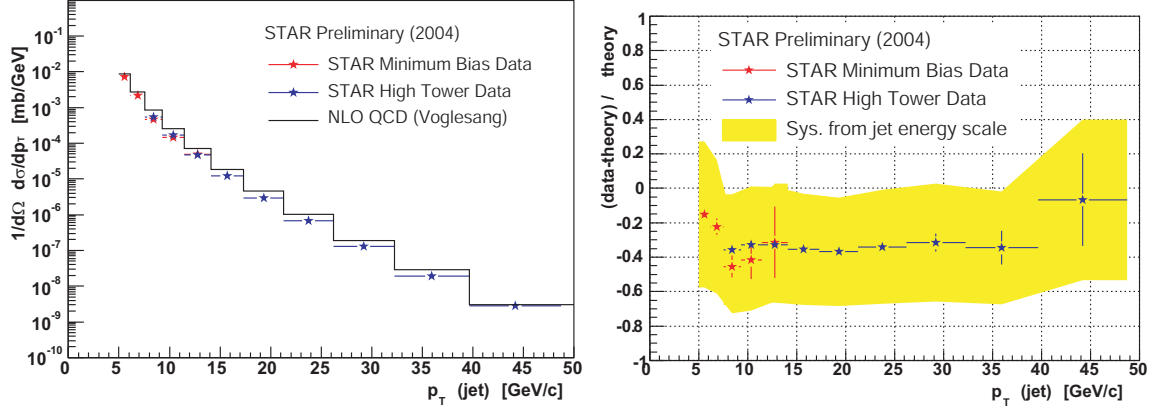


Figure 19. Preliminary corrected inclusive jet cross section from 2004 STAR data. The minimum bias and high tower trigger sets overlap for three bins in the region $7 < p_T < 12$ GeV/c. The NLO pQCD calculation¹⁰ has binning identical to that used for the data. The right-hand frame shows the fractional difference between the measured and predicted cross sections, with the yellow band representing the dominant systematic uncertainty due to present limitations on the precision of the jet energy scale.

The analysis of systematic uncertainties in the cross section results, including those in the aforementioned correction factors, is in progress. The yellow band in Fig. 19 represents what we judge to be the dominant uncertainty – $\sim 50\%$ in cross section arising from the present $\sim 10\%$ uncertainty in the jet energy scale. This is very similar to previous jet studies at CERN and FNAL. It is important to note that the energy scale systematic will be greatly reduced when additional *in situ* probes (such as γ -jet coincidences) become available with increased integrated luminosity in 2006. As seen in Fig. 19, the measured cross sections agree quite well in p_T -dependence with NLO pQCD calculations over 7 orders of magnitude, and agree marginally in absolute scale, within the present large systematic scale uncertainties. We find the general agreement at this stage of the analysis to be strongly encouraging, and to motivate the application of pQCD in interpreting our measured jet spin asymmetries.

2.3.2 Inclusive π^0 analysis status

In parallel with the jet analyses, significant progress has been made toward extraction of cross sections and A_{LL} for inclusive π^0 production in STAR over the pseudorapidity range $-1 < \eta < 2$. This work has not yet reached the stage of preliminary results, so we illustrate the progress here by means of reconstructed invariant mass spectra and projections of A_{LL} uncertainties for the endcap EMC. The EEMC was partially instrumented for the 2004 run, but fully instrumented and commissioned during 2005. Only the latter run has provided sufficient statistics to permit a meaningful tuning of parameters involved in the π^0 reconstruction algorithm, and this has begun within the last month.

Figure 20 shows a typical invariant mass spectrum reconstructed from photon pairs detected in the EEMC with a high-tower trigger, from a single day's data in the 2005 run,

and utilizing an EEMC relative calibration based on analysis of mip's in the detector. Photon candidates were identified by associating clusters of fired scintillator strips in the EEMC's shower-maximum detector (SMD) U- and V-planes into points. The total energy of each SMD point was determined from the energy response of the calorimeter towers in a 3×3 patch surrounding the point. In the event that multiple points share energy from a given patch of towers, that energy was divided between the points in proportion to the energy measured in the SMD planes. Pairs of photon candidates were then subjected to cuts to reject events where a photon initiated a shower before the endcap (as happens often in the support structure and cabling for STAR's Silicon Vertex Tracker). The kinematics of pairs that survive all cuts are determined assuming an event vertex provided by the TPC. The reconstructed π^0 peak mass has been used in previous analyses to determine the sampling fraction to be applied to the mip calibration, and is consistent here. The peak width (0.026 GeV) is presently $\sim 30\%$ larger than found in simulations that assume perfect calibration for all towers. While the dominant background shape drawn in Fig. 20 is empirical, simulations suggest that the spectrum shape can be very well understood without invoking backgrounds beyond combinatoric photon pairings (which can be estimated via mixed event analyses) and η^0 decay modes.

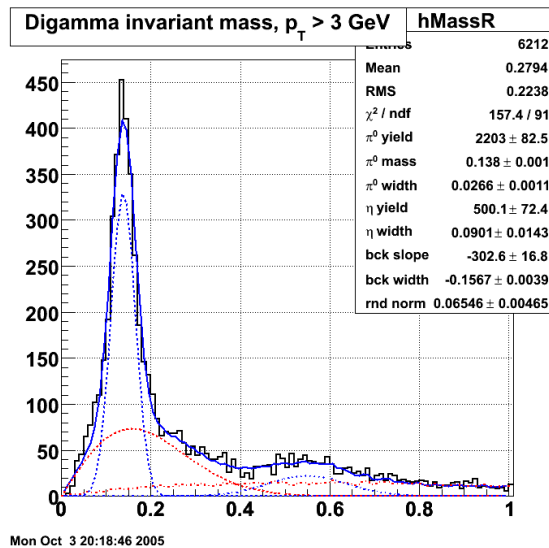


Figure 20. Invariant mass spectrum for reconstructed π^0 mesons measured in the EEMC from day 174 of the 2005 run.

Based on extrapolations from the 2005 data analyzed to date, Fig. 21 shows the A_{LL} statistical precision we expect to achieve for inclusive π^0 production in the EEMC alone from the 2005 run, together with the improvement foreseen from the proposed 2006 run. The improved integrated luminosity and polarizations will improve the figure of merit (FOM) for 2006 by a factor of 10 over that achieved in 2005. Anticipated experimental improvements will also increase FOM: shielding at STAR should increase the useful fraction of high tower triggers by 30%; a fast vertex position detector should allow at least 10% of all fast-detector triggered data to be analyzed with vertex resolution comparable to that provided by the TPC in slow-detector data, potentially doubling the data sample. Taken together, these factors will provide a factor ~ 25 boost in FOM over

2005, or a factor of 5 improvement in statistical uncertainties. Figure 21 does not include other anticipated improvements, such as Level 2 triggers that should greatly increase the trigger \times reconstruction efficiency near the high-tower threshold, and addition of SMD peak-fitting to the clustering algorithm, which should greatly slow the rate of deterioration seen in the uncertainties in Fig. 26 above $p_T \sim 10$ GeV/c.

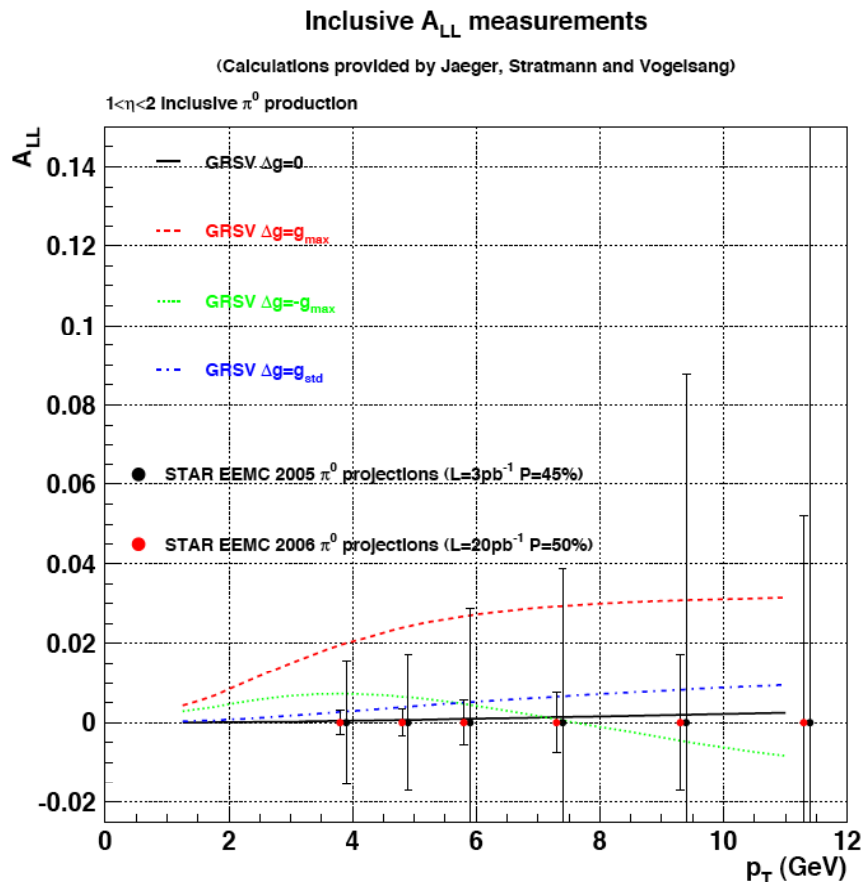


Figure 21. Projected A_{LL} statistical precision for inclusive π^0 production in the endcap EMC region from the 2005 vs. 2006 runs. Comparable uncertainties should be provided by the barrel EMC, whose full acceptance will be included in STAR's trigger for the first time in 2006.

Analogous π^0 reconstruction analyses for STAR's barrel EMC have been progressing for some time for d+Au data taken in 2003, and have recently begun for pp collisions as well. The SMD clustering approach for BEMC is different from that in EEMC because of the different nature of the shower-maximum detectors (gaseous for BEMC, plastic scintillator for EEMC). Figure 22 shows typical invariant mass spectra obtained. Since the focus to date has been on extraction of cross sections, which can proceed with lower yields, there has been less emphasis so far on optimization of reconstruction efficiency for BEMC. When this is done, it is anticipated that the barrel will contribute even more yield than the EEMC to STAR's 2006 π^0 sample for A_{LL} analyses, consistent with its larger acceptance. The combined data from the two subsystems should then provide a significant complement to the Δg discriminating power anticipated from the inclusive jet sample. Since the π^0 's are predicted to arise with little bias from both quark and gluon

jets, the two channels should show internal consistency if the effects of fragmentation are properly included in the theoretical calculations.

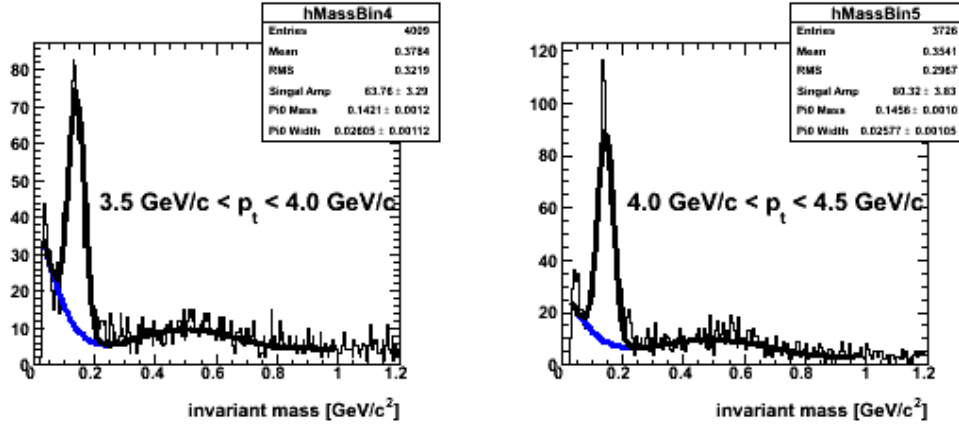


Figure 22. Reconstructed di-photon invariant mass spectra for two different p_T bins in the BEMC, applying an energy calibration determined from the p/E ratio for electrons tracked to the BEMC.

Optimization of π^0 reconstruction algorithms is viewed as an essential step along the path toward direct photon analyses, which will rely heavily on SMD transverse shower shape analysis, in addition to isolation cuts, to discriminate against π^0 's. The statistically robust sample of direct photons expected from the 2006 run (comparable, for example, to the 2005 sample of π^0 's in the endcap) will facilitate the development and tuning of such discrimination algorithms. Assuming reasonable reconstruction efficiencies, the A_{LL} uncertainties that should be provided by an inclusive direct photon sample in 2006 are very closely matched to the maximum (100% gluon polarization at initial scale) theoretical curve (red dashed) in the lower left frame of Fig. 14. Thus, 2006 inclusive photon A_{LL} results will not yet provide much discriminating power for Δg . Indeed, in the long run the greatest sensitivity from direct photon studies is expected to come from γ -jet coincidences, for which STAR's acceptance is optimized (by design) for regions of phase space where the spin asymmetries are expected to be largest, because both the quark polarizations and QCD Compton scattering spin correlation coefficient (\hat{a}_{LL}) are high. The proposed 2006 run would provide a critical start on that study.

2.3.3 STAR EMC calibration status

Procedures are by now well established for both barrel and endcap EMC's to allow online matching of gains of the many towers to $\sim\pm 10\%$ and offline determination of achieved gains to $\sim\pm 5\%$ precision. The procedures differ in the two cases, primarily due to the deterioration of TPC tracking resolution and availability in the endcap region. Relative gains are established first for all towers by analyzing mip spectra for both systems. For the BEMC, mip's depositing energy in a single tower are defined by means of TPC tracking and momentum measurement. For the EEMC the analogous mip identification

relies on the combined response of the tower, preshower, postshower and SMD subsystems of the calorimeter. The gains determined for each of the 720 EEMC towers in this way are shown in the left frame of Fig. 23, where comparison with the blue “goal lines” reflects the accuracy of online high voltage adjustments in 2005. The absolute scale of EEMC gains is adjusted to give the π^0 invariant mass at its correct value. The overall energy scale of the barrel towers is instead matched to the TPC, by comparing the measured tower response for $2 < E_T < 10$ GeV electrons (selected in the TPC) to their measured momenta, as illustrated by the p/E spectrum in the right frame of Fig. 23. As shown in Fig. 22, this electron calibration gives a π^0 peak mass typically within 5% of the correct value. The ultimate desired calibration precision for both EMC’s is under 2%, and reaching this goal will require more detailed analysis of invariant masses for several mesons, and understanding of small systematic discrepancies among calibrations made by different methods or under different beam conditions.

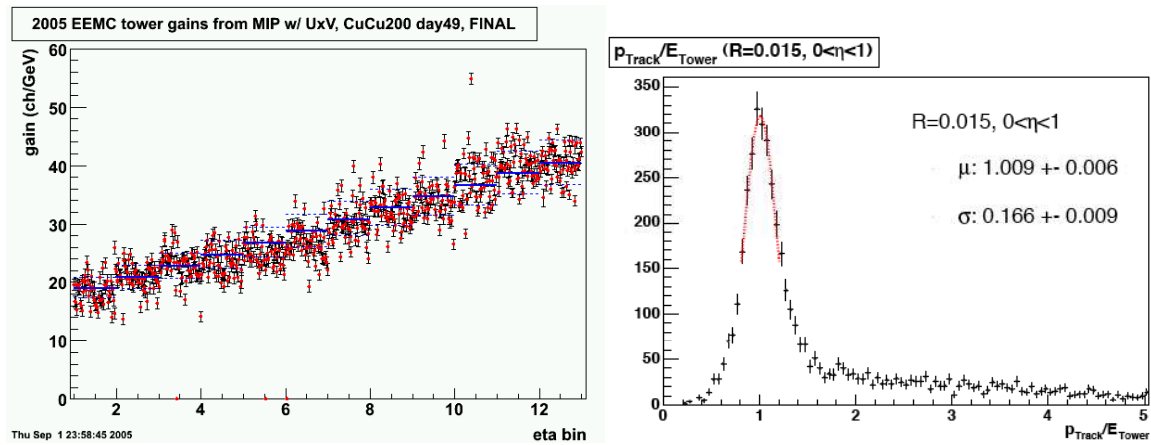


Figure 23. Stages in the energy calibration of STAR EMC’s. The left frame shows the gain determined for each of the 720 EEMC towers from the most probable energy deposition of mip’s selected by the combined response of all EEMC subsystems. The gains are shown vs. pseudorapidity bin for 2005 Cu+Cu data, in comparison with blue horizontal lines that define the goals (and $\pm 10\%$ deviations from the goal) set for matched E_T response. The right frame shows the distribution of p/E values for electron candidates tracked through the TPC to BEMC towers, after adjustment of the BEMC calibration scale.

2.4 Worldwide competition to determine gluon polarization

While RHIC has the opportunity to make unique contributions to the study of nucleon spin structure, there is also significant worldwide competition from lepton beam facilities to measure the polarization of gluons in a polarized proton. Polarized lepton-nucleon scattering experiments have so far been restricted to fixed-target experiments, resulting in a limited x and Q^2 coverage. The crude existing constraints on Δg come from study of scaling violations in polarized deep inelastic scattering, and these are likely to be significantly improved only with the advent of a polarized e-p collider, such as eRHIC. However, information on Δg over limited x -ranges is supplied more directly by the ongoing polarized fixed-target programs at HERMES (HERA) and COMPASS (CERN). These experiments focus on photon-gluon fusion, $\gamma^* g \rightarrow q\bar{q}$, enhancing this gluon-sensitive process by detecting either open charm or moderate-to-high p_T hadron pairs in

the final state. As revealed in Fig. 24, they have currently attained precision levels comparable to those in the STAR and PHENIX spin programs, and they are expected to keep apace until RHIC has accumulated a major portion of its integrated luminosity goal for 200 GeV pp running.

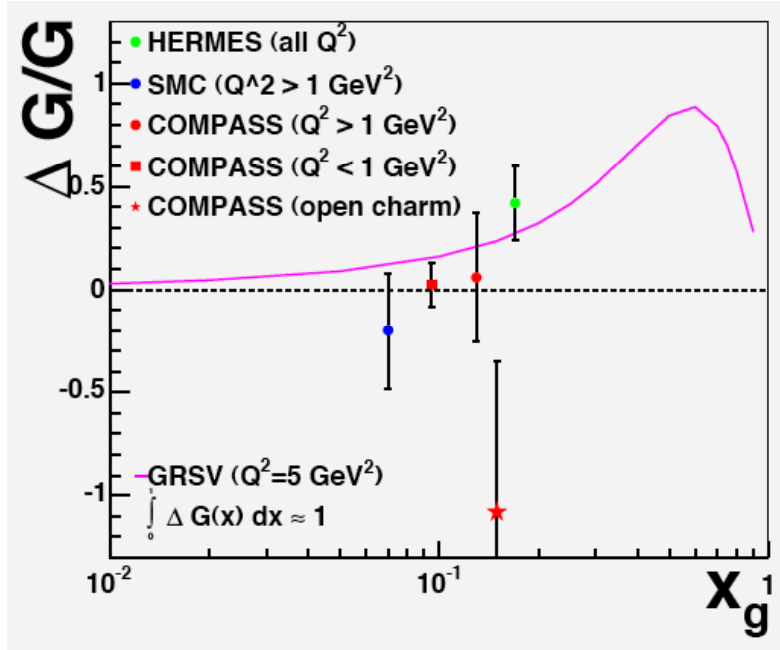


Figure 24: Measurements of $\Delta g / g$ in lepton-hadron production as a function of x_g .

The most robust competition comes from the COMPASS (Common Muon and Proton Apparatus for Structure and Spectroscopy) collaboration at CERN, which is studying lepto-production of open charm and hadron pairs with large transverse momentum. Figure 24 shows COMPASS results for $\Delta g / g$ from data collected in 2002 and 2003, compared to the same GRSV (standard solution) parameterization of gluon polarization shown in STAR projections above (e.g., the black curve in Fig. 15) and to earlier $\Delta g / g$ results obtained by SMC and HERMES from lepto-production of high- p_T hadron pairs. The measurements cluster around $x \approx 0.1$ and span a broad range in $\Delta g / g$. But clearly COMPASS will shortly rule the lepto-production roost (the HERMES program will be terminated by summer 2007, and will focus on transverse and nuclear spin effects until then). It will be some time before the theoretically clean charm production channel provides statistically interesting results, but the addition to Fig. 24 of COMPASS data collected in 2004 and anticipated in 2006 should yield a discriminating measurement via the hadron pair production channel. The long pp run proposed herein for 2006 would nonetheless push the RHIC spin program into the forefront of this field at an opportune moment.

The RHIC spin program has long-term advantages over fixed-target lepton-nucleon experiments for gluon polarization determination, resting on three features: 1) access to much higher momentum transfers, where pQCD should work best; 2) coverage of a much broader range in x_{gluon} , permitting constraints on the integral gluon contribution to proton spin; 3) access to several relevant reaction channels, with differing sensitivity and experimental systematic concerns, to test the robustness of the pQCD interpretation of the results. Since the pp and lepton-nucleon measurements will cover quite different regions in Q^2 , and the gluon distributions evolve substantially with Q^2 , eventually both types of data will be needed as input to a global NLO pQCD analysis to extract optimal constraints on gluon helicity preferences in a longitudinally polarized proton.

2.5 Transverse Spin Physics Goals

During Run 2, STAR found [1] large transverse single-spin asymmetries for inclusive π^0 production at $\eta = 3.8$ and large x_F , as shown in Fig. 25. The STAR results are similar to previous measurements by the FNAL E704 collaboration for p+p collisions at $\sqrt{s} = 20$ GeV¹¹. However, as shown in Fig. 25, STAR has also demonstrated that the cross section for large rapidity inclusive π^0 production in p+p collisions at RHIC is consistent with expectations from pQCD [1], in contrast to the situation at lower \sqrt{s} ¹². Thus, the RHIC results are the first time that large transverse single-spin asymmetries have been observed in p+p collisions a kinematic region where pQCD appears to be applicable. Transverse single-spin asymmetries that are significantly different from zero have also been reported recently in semi-inclusive deep-inelastic scattering measurements¹³. The intrigue surrounding these results has sparked a number of experiments to study the unexpectedly large signals. For example, the HERMES collaboration has devoted significant effort to measure semi-inclusive DIS with a transversely polarized target¹⁴. In addition, COMPASS is planning to run with a transversely polarized proton target next year to confront the HERMES results.

These results have stimulated a great deal of interest toward understanding transverse spin effects in QCD. Different mechanisms have been identified in the pQCD framework by which one might expect transverse spin effects by removing restrictions of the collinear, factorized, leading-twist framework. The Sivers model adds explicit k_T dependence to the parton distribution functions. In this case, a non-zero A_N can arise from correlations between the nucleon spin and the parton k_T that vanish unless partons carry orbital angular momentum. The Collins model attributes single-spin effects to the convolution of the transversity distribution function with a spin-dependent fragmentation function that adds explicit k_T dependence to the fragmentation process. Instead of introducing k_T dependence in either the parton distribution or fragmentation functions, others have studied collinear twist-3 effects and found 2 terms that correspond to the Sivers and Collins effects.

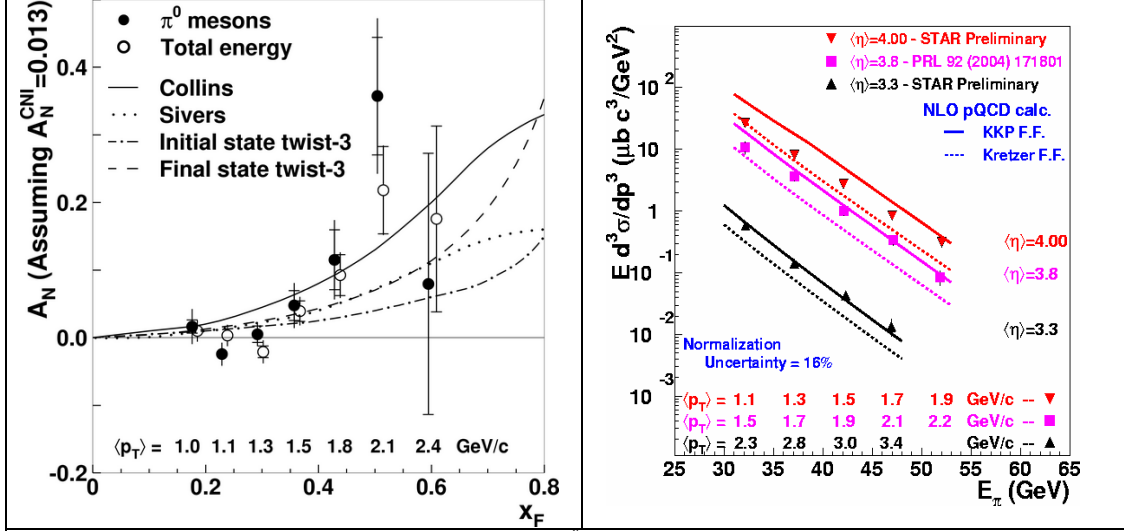


Figure 25: The left panel shows A_N for inclusive π^0 production at $\eta = 3.8$ [1]. The right panel shows the comparison between the measured cross section for inclusive π^0 production at forward rapidity and predictions from pQCD calculations using two fragmentation functions.

Exploring these transverse spin effects represents an extremely important complement to the gluon polarization measurements that are the focus of the current longitudinal polarization measurements. The Siverson mechanism provides a window to explore parton orbital angular momentum. In addition to the gluon spin, parton orbital angular momentum is another place where the missing spin of the “spin crisis” may be found. The large single-spin asymmetries seen in p+p collisions and semi-inclusive DIS may be giving a first hint of non-zero parton orbital angular momentum. Meanwhile, the Collins mechanism provides a way to measure transversity in the nucleon. The transversity distribution, $\delta q(x)$, measures the tendency of a quark to have its spin parallel to that of a transversely polarized proton. This is the last unknown leading twist-2 quark distribution. The transversity distribution, $\delta q(x)$, and the longitudinal polarization, $\Delta q(x)$, are not trivially related because boosts and rotations do not commute. Unlike the longitudinal polarization, the gluons in the nucleon make no contribution to the transversity distribution. Thus, the difference between these two distributions carries important information about the non-perturbative structure of the proton. Measurements of the transversity are also important to compare with lattice QCD results for the tensor charge of the nucleon.

STAR has continued its study of transverse single-spin asymmetries during the brief transverse spin running periods in Runs 3 and 5. Additional data have been taken at mean pseudorapidities of 3.7 and 4.0 as shown in Fig. 26, which begin to permit a separation between the x_F and p_T dependence of the effects. Notably, we find A_N is consistent with zero in the negative x_F region. According to a recent study, the large negative x_F region is dominated by the gluon Siverson¹⁵ function. Meanwhile, the data are consistent with the $1/p_T$ dependence expected in pQCD, but the precision is not yet sufficient to draw a definite conclusion.

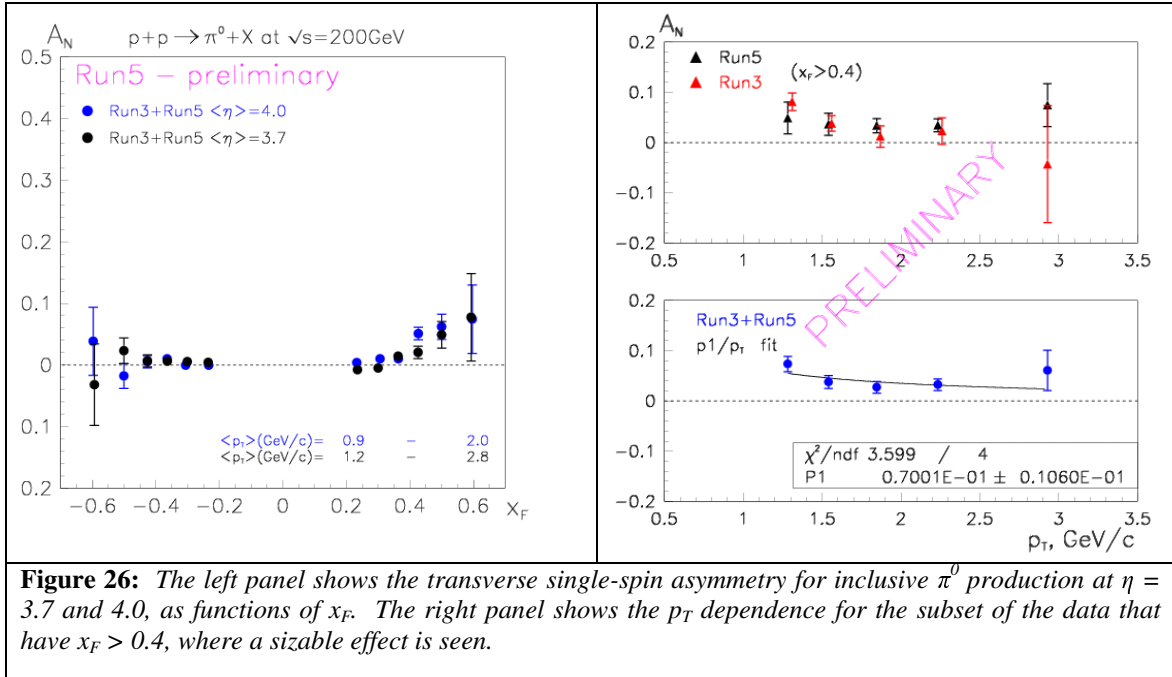


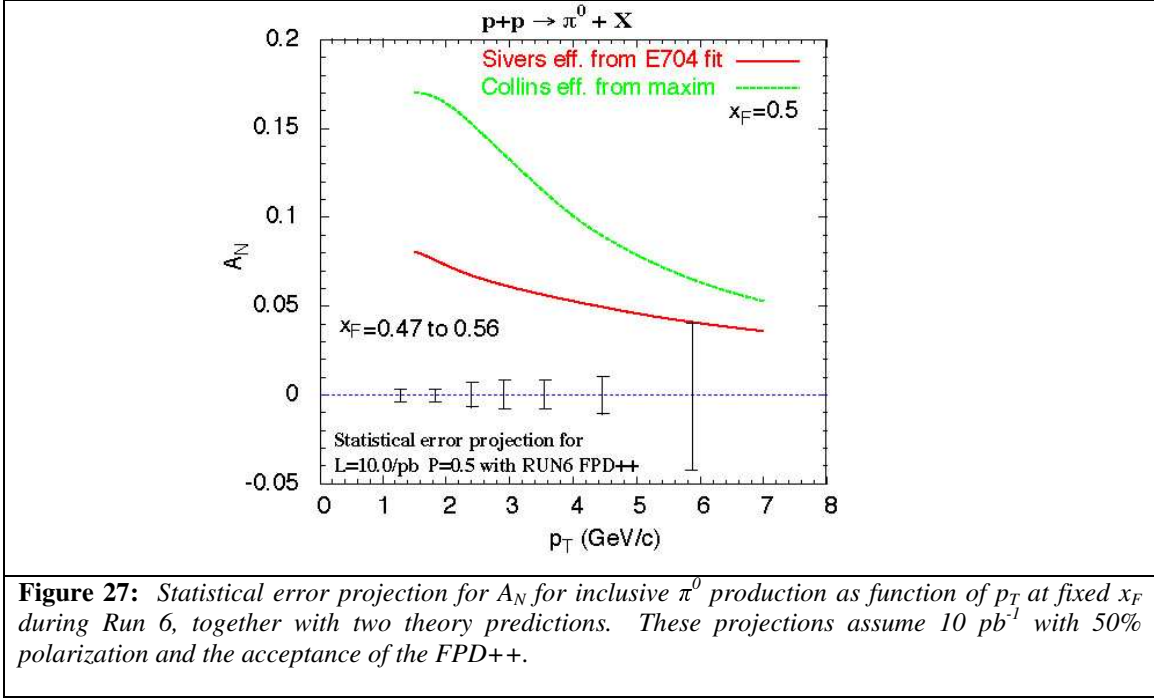
Figure 26: The left panel shows the transverse single-spin asymmetry for inclusive π^0 production at $\eta = 3.7$ and 4.0 , as functions of x_F . The right panel shows the p_T dependence for the subset of the data that have $x_F > 0.4$, where a sizable effect is seen.

The FPD++ will dramatically increase the STAR acceptance for detecting large rapidity π^0 . The impact of this is illustrated in Fig. 27, which shows the projected statistical error for A_N that STAR will achieve as a function of p_T for a *single* x_F bin during the proposed Run 6. The high precision (x_F , p_T) decomposition of the large rapidity transverse single-spin asymmetries will provide a significant step forward in our understanding of this process. Obtaining precise data for very large x_F will also be valuable to test the expectation that A_N should decrease at sufficiently large x_F ¹⁶, due to the Soffer inequality¹⁷ bounding the transversity distribution function.

However, to disentangle the different mechanisms behind the single-spin asymmetries fully, we must go beyond inclusive π^0 measurements. The characteristic difference between the Sivers and Collins effects is that the former represents a spin asymmetry in jet production, whereas the latter involves a spin asymmetry in jet fragmentation about the thrust axis. STAR will exploit the much larger acceptance of the FPD++, when compared to the FPD, to perform two measurements that are designed to distinguish between these two effects.

The FPD++ is sufficiently large that we will be able to search for coincident particles within a jet cone of radius $> \sim 0.5$ whenever a π^0 is detected within the central 6x6 array of small Pb-glass crystals. Jet-like events including at least one additional photon in coincidence with the π^0 will be observed in $>10\%$ of the inclusive π^0 events. This will permit us to measure A_N for the jet-like events with considerably better precision than we have been able to achieve to date for inclusive π^0 . A non-zero value will be a clear indication of a Sivers contribution. We will also measure the relative orientation of the π^0

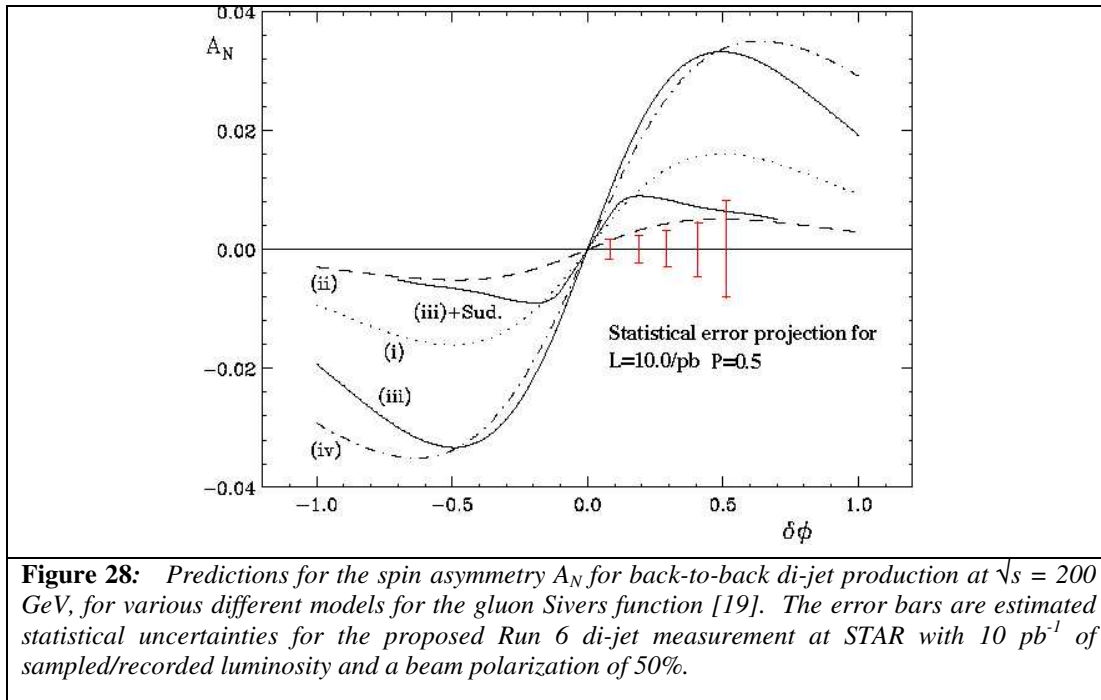
and the additional photon(s) about the thrust axis. In this case, an asymmetry would be a clear signature for the Collins effect.



The FPD, which consists of 7×7 arrays of small Pb-glass crystals identical to those in the center of the FPD++, has already demonstrated excellent ability to distinguish between events that include 1 or 2 photons. But most of the single-photon events in the FPD arise from π^0 decays where the second photon falls outside the 7×7 array. In contrast, the FPD++ is sufficiently large that it will detect $> 95\%$ of the second photons from π^0 decay when the first photon deposits > 25 GeV in the 6×6 array. Thus, it will be an excellent tool to identify the direct photon events through isolation cuts around a photon cluster. Simulations indicate that we will detect $\sim 100\text{K}$ direct photons with $E > 25$ GeV ($\langle p_T \rangle \sim 2.3$ GeV/c) within a fiducial region during a 10 pb^{-1} run. The single-spin asymmetry A_N for these direct photons is sensitive to the large- x quark Sivers function, and includes no contribution from the Collins effect¹⁸.

It is also important to explore whether or not k_T dependent parton distribution or fragmentation functions may play a role at mid-rapidity. Ideally, one should study an observable with leading-order sensitivity to a small k_T value, while still introducing a large scale Q so that pQCD can make reliable predictions. One such observable, back-to-back di-jet production in transversely polarized p+p collisions, can be used to measure the Sivers function¹⁹. The deviation of the azimuthal angle difference $\delta\phi = \phi_{jet1} - \phi_{jet2} + \pi$ from zero directly measures the k_T of the colliding partons. When one of the jets has its thrust axis oriented along the spin of the nucleon, the k_T imbalance of the parton distribution associated with the Sivers effect will modify the $\delta\phi$ distribution and produce a spin-dependent asymmetry. STAR is an ideal detector to measure this effect. The full azimuthal acceptance and large pseudorapidity coverage permit complete jet

reconstruction over a large phase space. This allows a clean separation between the Sivers effect of interest and the Collins effect, which may produce an asymmetry if only hadron fragments are observed. Furthermore, STAR will measure di-jet events with the average thrust axis along the spin direction and di-jet events with the average thrust axis perpendicular to the spin direction simultaneously. This will permit a detailed investigation of any instrumental asymmetries that may be present, as the latter should have no $\delta\phi$ asymmetry. At mid rapidity, this asymmetry may reach a few percent or more and provides access to the gluon Sivers function. Figure 28 shows predictions for the magnitude of the effect. Superimposed are error bars indicating the estimated statistical uncertainties for a di-jet measurement at STAR with 10 pb^{-1} and 50% beam polarization during Run 6. This measurement will profit dramatically from the L2 trigger improvements to enhance di-jet yields that are underway. Without those, STAR would need to integrate ~ 4 times the proposed Run 6 transverse figure-of-merit in order to achieve the same final precision.



2.6 Low Energy Au+Au Collisions: the Onset of Hydrodynamic Behavior

If machine performance and improvements in detector efficiency permit the transverse and longitudinal spin goals proposed by STAR to be completed sufficiently early, STAR proposes short Au+Au runs at two energies, $\sqrt{s_{NN}} = 19.6$ and 31 GeV, to complete the energy scan for soft physics observables.

Some of the most exciting results from the first years of RHIC data taking involve the measurement of the azimuthal anisotropy parameter v_2 (elliptic flow). The striking

agreement for various particle species between the $v_2(p_T)$ observed experimentally and the predictions of hydrodynamics at low transverse momenta is taken as strong evidence for local thermalization in a possible new state of matter.

In Au+Au collisions at the higher RHIC energies ($\sqrt{s_{NN}} = 130$ and 200 GeV), v_2 is found to be as large as predicted by hydrodynamic models while at top SPS energy (17.2 GeV), measurements show that $v_2(p_T)$ is substantially smaller. RHIC has also collided Au ions at $\sqrt{s_{NN}} = 20$ and 62.4 GeV. At 62.4 GeV, $v_2(p_T)$ is found to be similar to $v_2(p_T)$ at 200 GeV. The bottom panels of Figure 29 show $v_2(p_T)$ at 17 and 200 GeV scaled by $v_2(p_T)$ at 62.4 GeV for various identified particles. The data sample taken by the STAR experiment at 20 GeV was too small to be used in these plots. The plots demonstrate that $v_2(p_T)$ changes significantly from 17 GeV to 62.4 GeV but that the shape and magnitude of $v_2(p_T)$ at higher energies is comparatively stable.

The experimental observation of limiting behavior in an observable like v_2 can convincingly demonstrate the validity of a zero mean-free-path approximation and the attainment of a hydrodynamic limit. The STAR collaboration therefore places high priority as a secondary goal on precision measurements of $v_2(p_T)$ at $\sqrt{s_{NN}} = 19.6$ and 31 GeV. The RHIC facility has the unique ability to perform an energy scan that encompasses the apparent transition to a perfect fluid-like behavior of quarks and gluons during the early stage of heavy ion collisions at 200 GeV. STAR requests 1 week of data taking at 19.6 GeV and 1 week of data taking at 31 GeV. Measurements at these energies will focus on low p_T observables rather than rarer probes. Measurements of particular interest include $v_2(p_T)$ for identified particles, HBT radii, $\langle p_T \rangle$ fluctuations, and the higher harmonics of the azimuthal anisotropy (v_4, v_6, \dots).

An energy scan may also provide indirect evidence for a possible saturated gluon density (Color Glass Condensate (CGC)) in the initial state wave function of Au nuclei in $\sqrt{s_{NN}} = 200$ GeV collisions. The resulting change in the x Bjorken range relevant for particle production at mid-rapidity makes possible effects due to a CGC much less likely; changes in particle production related to this may be observable. Experimental tests to determine the possible existence of a CGC are of great interest, especially given the recent theoretical interest in developing a CGC+Hydro+Cascade model for heavy ion collisions. A “discovery” measurement to test this hypothesis directly is proposed for run 7 by STAR using a newly commissioned Forward Meson Spectrometer (FMS) to search for mono-jets in d+Au collisions.

3. Proposal for RHIC Run VII (2006-2007)

For Run VII, assuming 29 weeks of cryo operation, STAR proposes 11+3 weeks of d+Au running and 10+3 weeks of running with polarized proton-proton collisions. The data acquired in the d+Au run will allow a definitive search for evidence of the saturated gluon density (Color Glass Condensate-CGC) predicted to exist in the initial state of relativistic heavy nuclei. The proton run, possibly with beams of longitudinally polarized protons, will provide essential reference data for the d+Au measurement preceding it, as

well as additional progress toward mapping the gluon polarization as a function of Bjorken x by measuring $\gamma + \text{jet}$ coincidences.

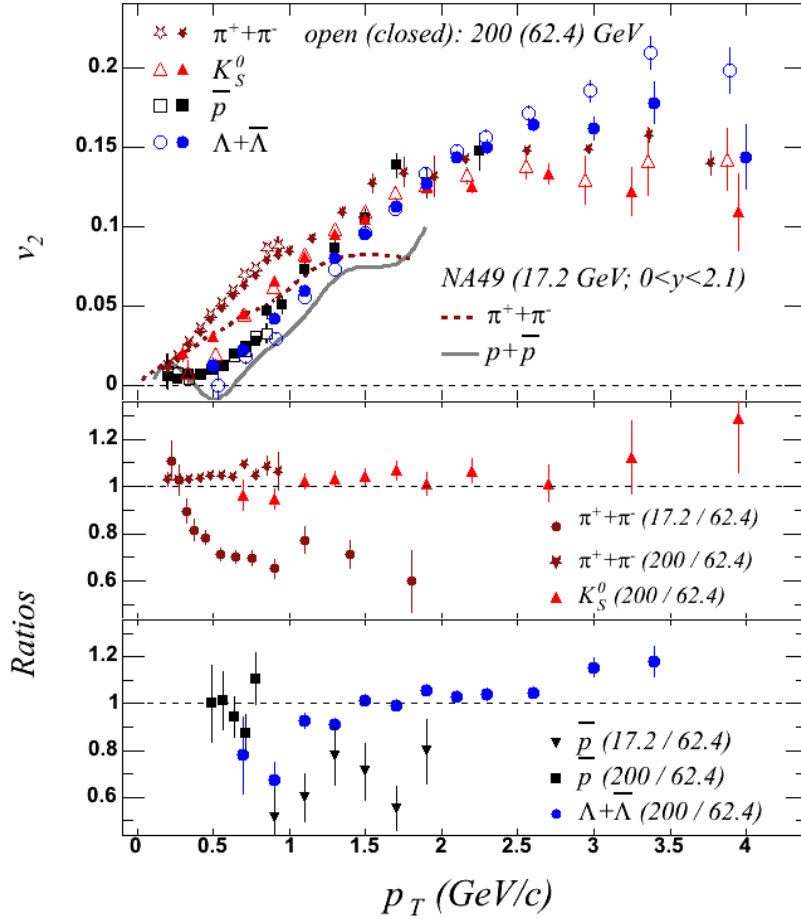


Figure 29. Top: Elliptic flow $v_2(p_T)$ as a function of p_T for various particle species measured at $\sqrt{s_{NN}} = 200, 62.4 \text{ GeV}$ at RHIC and $\sqrt{s_{NN}} = 17.2 \text{ GeV}$ at the CERN SPS. Bottom: ratios for various particle species of the $v_2(p_T)$ measure at the SPS and RHIC as a function of p_T

3.1 d+Au: the search for gluon saturation (Color Glass Condensate) in heavy nuclei

Measurements of inclusive particle production in d+Au collisions at RHIC have established that the yield of produced particles systematically decreases as their rapidity increases. These d+Au results suggest that the low- x gluon density in the gold nucleus at RHIC energies may be saturated. However, alternate explanations of the observed suppression have been offered, so evidence of gluon saturation at RHIC energies is not yet conclusive. Unambiguous determination of the gluon density in a heavy nucleus requires going beyond inclusive particle production to explore particle correlations in order to elucidate the dynamics that underlie the observed suppression of the inclusive yields. Perturbative QCD is known to describe inclusive hadron yields at forward rapidity in p+p collisions at RHIC (e.g., see Fig. 25). In pQCD, triggering on particle production

in the forward direction implies that the quarks from the deuteron beam are the predominant probes of the gluons in the Au nucleus. The gluon density in the Au nucleus is probed at the lowest Bjorken x values when pairs of jets, or their hadronic surrogates, are both observed at large rapidity.

It is important to quantify whether the gluon density in the Au nucleus saturates at RHIC energies. Knowledge of the quark and gluon distributions in the gold nucleus is essential for understanding the initial state of a Au+Au collision, and how that state evolves on apparently very short time scales into a strongly interacting quark gluon plasma. We know that most of the mass of protons and neutrons arises from the very strong color fields carried by the gluons that bind the nearly massless up and down quarks. But, we have essentially no knowledge about the gluon density in a heavy nucleus. It is expected that at the LHC a saturated gluon density will be manifest in p+p collisions in forward particle production and in ion collisions over the entire rapidity range, so it is timely to quantify the role of gluon saturation at RHIC prior to the start of operations of the LHC.

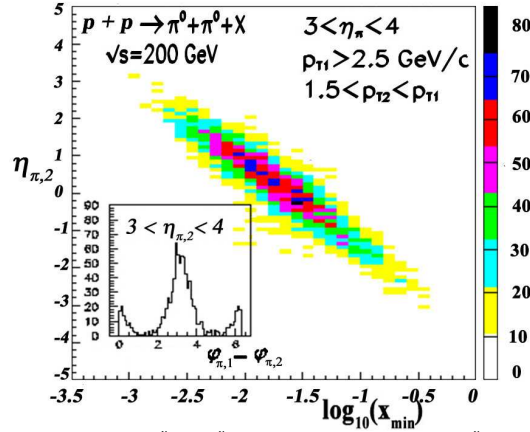


Figure 30. Pythia simulation of $p+p \rightarrow \pi^0 + \pi^0 + X$ with one of the π^0 detected in the region $3 < \eta < 4$ with $p_T > 2.5$ GeV/c, and the second π^0 detected with $p_T > 1.5$ GeV/c. The figure shows the correlation between the pseudorapidity of the second π^0 and the x of the struck gluon, while the inset shows the back-to-back azimuthal distribution.

The low- x gluon density in the Au nucleus can be measured in d+Au collisions at RHIC through correlated particle measurements. In pQCD, *inclusive* forward particle production in high energy hadronic collisions probes the gluon density over a broad range of Bjorken x values²⁰. The x value can be much better constrained through measurement of back-to-back pairs of particles. When an away-side hadron is detected in coincidence with a leading hadron or jet at forward rapidity, the pseudorapidity of the recoil jet or its hadronic surrogate reflects the x value probed. This is illustrated for p+p collisions in Fig. 30. The lowest x values are reached when both particles are detected in the forward direction.

If the suppression of the inclusive hadron yields at forward rapidity arises from effects such as leading-twist shadowing or incident parton energy loss, then the correlated back-to-back peak characteristic of $2 \rightarrow 2$ partonic scattering should still be present in d+Au

collisions²¹. In contrast, if the gluon density reaches saturation at RHIC energies, then it is expected that the quark from the deuteron beam will interact with multiple gluons from the Au nucleus. Hence, particle production will no longer be dominated by a single quark-gluon interaction and the pseudorapidity distribution of particles that balances the p_T of the forward particle production will be modified. The away-side peak in the $\Delta\phi$ distribution that signifies parton elastic scattering will be broadened or will disappear due to the multiple collisions the quark experiences if the gluon density in the gold ion reaches saturation²². Preliminary results from STAR as shown in Fig. 31 are suggestive that this disappearance may occur²³, but a far more detailed study is required in order to draw a firm conclusion.

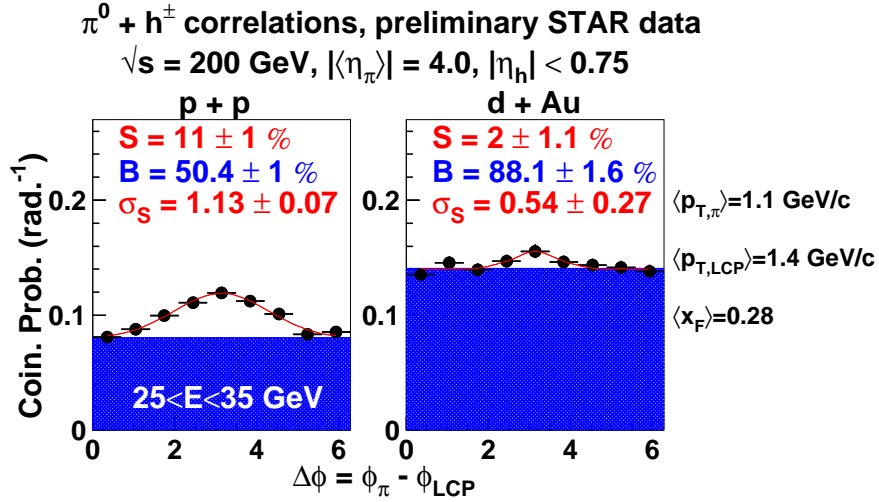


Figure 31. Preliminary azimuthal distributions of leading charged hadrons in 200 GeV p+p and d+Au collisions at mid-rapidity ($|\eta| < 0.75, p_T > 0.5 \text{ GeV}/c$) in coincidence with identified π^0 at $\langle\eta\rangle=4.0$.

A Forward Meson Spectrometer (FMS) (Fig. 32) is being added to STAR to enable measurement of the gluon densities in the Au nucleus down to x values where saturation is expected to become apparent. The FMS will span the pseudorapidity interval $2.5 < \eta < 4.0$. When the FMS is complete in the fall of 2006, STAR will have nearly hermetic electromagnetic calorimetry over the range $-1 < \eta < 4$. This broad coverage will enable the mapping of the nuclear gluon density down to $x \sim 0.001$ utilizing particles with sufficiently high p_T that the corresponding p+p collisions are well described by pQCD.

To quantify the role of gluon saturation at RHIC energies, it is timely to have a second d+Au run during RHIC Run 7. Detailed simulations have established that STAR can map out the gluon density in the gold nucleus over the range $0.001 \leq x \leq 0.3$ in a 10-week physics run of d+Au collisions at $\sqrt{s_{\text{NN}}} = 200 \text{ GeV}$, assuming the same machine performance as achieved in the last d+Au run. The spatial dependence of the gluon density in the Au nucleus will be determined by measuring the effective impact parameter of the triggered collisions. Both the STAR beam-beam counters and the forward time projection chamber will be used to measure particle multiplicities in the Au beam direction thereby constraining the impact parameter of the collision.

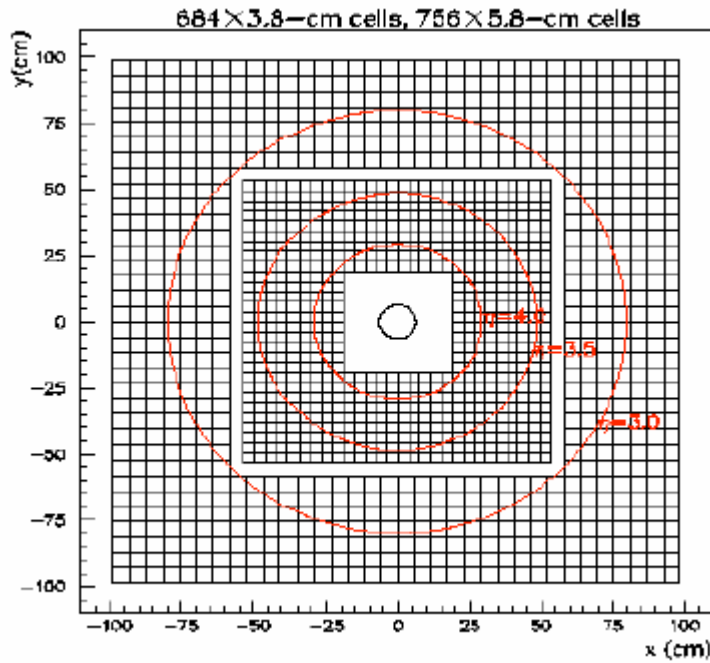


Figure 32. Front view of the layout of the Pb-glass counters comprising the FMS at STAR. The detector will greatly expand the acceptance for mesons decaying to photons and for meson coincidences in a kinematic region dominated by contributions from gluons at low x Bjorken. The pseudorapidity coverage is indicated by the red circles representing loci at $\eta = 3.0, 3.5,$ and 4.0

3.2 p+p: reference data for the CGC; progress in mapping the helicity preference of gluons as a function of x Bjorken

A 10 week physics run of p+p collisions at $\sqrt{s_{NN}} = 200$ GeV following the addition of the FMS to STAR is required to provide reference data to establish nuclear modifications of the gluon density.

This data will be useful as well to make continued progress on the spin physics measurements requiring high polarization and large integrated luminosity. The distribution of beam time between running with transverse and longitudinal polarization will be informed by progress in run 6. However, a clear priority will be to make progress toward obtaining a statistically meaningful sample of γ -jet coincidence events to further the analysis of that crucial channel. Acquisition of sufficient γ -jet statistics to reach the STAR goal of determining $x\Delta g(x)$ to $\sim \pm 0.1$ in each of several $\ln(x)$ -bins will require ~ 90 pb^{-1} of sampled cumulative luminosity at an average beam polarization $\sim 65\%$. This goal is sufficiently challenging that integration of data from several running periods will be required.

It is expected that in run 6, progress will be made with transverse polarization towards determining the origin of the large spin asymmetry observed in the production of forward π^0 mesons from transversely polarized protons. This will help to quantify the degree to

which orbital motion of quarks and/or gluons contributes to the spin of the proton. The need for additional transverse running will be assessed based on preliminary results from Run 6.

4. Proposal for RHIC Run VIII (2007-2008)

For Run VIII, assuming 29 weeks of cryo operation, STAR proposes 15+3 weeks of Au+Au running and 6+3 weeks of running with polarized proton-proton collisions. The data acquired in the Au+Au run will allow precision tests of the properties of quark-gluon matter, and a search for evidence of chiral symmetry restoration e.g. by studying leptonic decays of light vector mesons. Assuming sufficient progress in Runs VI and VII, the proton run will likely constitute the conclusion of $\sqrt{s} = 200$ GeV running dedicated to mapping the gluon polarization as a function of Bjorken x by measuring $\gamma + \text{jet}$ coincidences. Further data with $\sqrt{s} = 500$ GeV will then be needed to extend the measurement of $\Delta g(x)$ to the lowest accessible x Bjorken accessible at RHIC in order to reduce uncertainties from extrapolating into this region.

The near-term upgrades planned by STAR are a Forward Meson Spectrometer, a barrel TOF detector, DAQ1000 upgrade, and a micro-vertex detector. For Run VIII STAR expects to have the complete FMS (Run VII), the complete DAQ1000 upgrade, half of the TOF barrel detector, and a prototype micro-vertex detector.

These upgrades will improve the performance of the STAR detector significantly by Run VIII (in some cases by an order of magnitude). For that reason, the Collaboration is firmly convinced it is most effective to defer the next long Au+Au run until these upgrades are substantially complete, making a strong advance in the interim on measuring $\Delta g(x)$ and searching for the CGC in Runs VI and VII respectively. Some simple examples illustrate this point.

Based on simulations and demonstrated performance of the multi-gap resistive plate chambers that will be used for the TOF barrel detector²⁴, the reduction e.g. in the number of events required to obtain a statistically robust dataset for various charm particles and resonances is indicated in Table II for selected p_T ranges by the Figure of Merit (FOM).

From Table II for example one observes that once the TOF upgrade is substantially completed, the number of events required to obtain a 3σ signal in the invariant mass distribution for D^0 mesons decreases by a factor of ~ 5 ; for the strange resonance $\Lambda(1520)$ as well as other charm states (e.g. D_s^+) the reduction in the number of events required is over an order of magnitude. For reference, in Run IV, 50M events were required (acquired over 10-15 weeks) to obtain a 5σ signal using a brute force combinatoric subtraction procedure. The qualitative improvement provided in this one instance alone will open entirely new research horizons: the possibility to study possible charm thermalization; the possibility to study strange resonances in medium to test the mechanism of hadronization and the effect of the medium on dissociation and regeneration of such states.

The combination of TOF information with specific ionization (dE/dx) information in the TPC will provide the ability to cleanly identify electrons out to ~ 3 GeV/c. This capability combined with the large acceptance of STAR will allow detection of the leptonic decays of vector mesons to search for evidence of chiral symmetry restoration. This capability will also dramatically improve STAR's ability to measure non-photonic electrons from charm semi-leptonic decays, a key measurement for testing the coupling of charm quarks to the produced matter, and by extension, whether the matter is partonic.

Table II

| | p_T (GeV/c) | FOM |
|-----------------|------------------|------|
| D^0 | All | 4.6 |
| D^0 | 2-4 | 2.6 |
| D^0 | 4-6 | 2.0 |
| D^0 | >6 | 1.0 |
| K_0^* | 0-1 | 2.0 |
| K_0^* | 1-2 | 1.85 |
| K_0^* | 2-3 | 1.74 |
| K_0^* | 3-5 | 1.39 |
| $\phi(1020)$ | 0-2 | 5.0 |
| $\phi(1020)$ | 2-5 | 3.4 |
| $\Lambda(1520)$ | 0-1.6 | 11.4 |

Table II For various particle species as a function of transverse momentum range, the reduction (FOM) in the number of events needed to obtain a 3σ signal with and without the STAR TOF upgrade

The hadron identification capabilities of the TOF over a large fraction of the full 2π STAR acceptance, combined with the a newly implemented DAQ1000 ability to gather data an order of magnitude faster will allow the intermediate p_T region to be probed with unprecedented precision and in detail. Correlation measures revealing complex structures in this p_T regime are already hinting at details of the dynamic evolution of the produced matter (c.f. Figs 8-10): these structures likely result from an interplay between the flowing medium, jet remnants, and the coalescence of constituent quarks into final-state hadrons. Hadron identification over a substantial portion of the high statistics correlation space possible with these upgrades will afford information key to disentangling the role of these effects.

Short wavelength (rare) probes such as measurement of the upsilon family of states, high p_T direct photons, and direct photon + jet coincidences will benefit significantly from the DAQ1000 upgrade which, by increasing the available DAQ throughput by an order of magnitude, will afford zero dead-time data acquisition for such probes. This means STAR will be able to sample the full RHIC luminosity resulting in an increase in

throughput for triggered rare probes of a minimum of a factor two compared to present operation.

For reasons such as these, the STAR Collaboration is firmly convinced the most effective use of the RHIC beam demands deferring the next long Au+Au run until these upgrades are substantially complete. In addition, the long p+p run proposed for Run VI will provide C-AD the opportunity to continue machine developments, such as the commissioning of the cold snake in the AGS, to improve the luminosity and polarization further. These developments are essential in order to achieve the ultimate STAR goal for 200 GeV running – a direct measurement of the momentum-dependence of the gluon polarization, $\Delta g(x)$, over a broad x range via the γ +jet channel.

5. Collaboration Readiness

The STAR Operations Group, as well as the STAR Collaboration membership have been participating in an extensive program of shut-down activities in preparation for Run VI, including the installation of an engineering prototype of the Forward Meson Spectrometer, named the FPD++. STAR will be fully prepared to begin the program outlined for Run VI.

The complete Forward Meson Spectrometer will be operational in time for Run VII.

Steady progress is being made toward starting the construction of the TOF barrel upgrade that will be substantially implemented in time for a high statistics Au+Au run in FY08. The DAQ1000 upgrade, which will increase STAR's data acquisition throughput by an order of magnitude will be operational by run 8 as well. A prototype of a new micro-vertex detector designed to operate in tandem with the existing Silicon Strip Detector (SSD) is also planned to be tested during this beam time.

¹ J. Adams et al. (STAR Collaboration), Phys. Rev. Lett. **92**, 171801 (2004).

² B. Muller and K. Rajagopal, "From entropy and jet quenching to deconfinement?," arXiv:hep-ph/0502174.

³ M. Glück, E. Reya, M. Stratmann and W. Vogelsang, Phys. Rev. **D63**, 094005 (2001).

⁴ S.S. Adler, *et al.* [PHENIX Collaboration], Phys. Rev. Lett. **91**, 241803 (2003); K. Okada [PHENIX Collaboration], arXiv:hep-ex/0501066.

⁵ J. Adams, *et al.* [STAR Collaboration], Phys. Rev. Lett. **92**, 171801 (2004); G. Rakness [STAR Collaboration], arXiv:nucl-ex/0501026.

⁶ L.C. Bland, in EPIC99 Proceedings, eds. L.C. Bland, J.T. Londergan and A. Szczepaniak (World Scientific, Singapore, 2000), and arXiv:hep-ex/9907058.

⁷ *Research Plan for Spin Physics at RHIC*, BNL Report submitted to DoE, February 2005 (see Fig. 16).

⁸ T. Gehrman and W.J. Stirling, Phys. Rev. **D53**, 6100 (1996).

⁹ M. Miller [STAR Collaboration], contributed talk at Hawaii DNP meeting, Sept. 2005; J. Kiryluk [STAR Collaboration], invited talk at Hawaii DNP meeting, Sept. 2005.

-
- ¹⁰ B. Jager, M. Stratmann and W. Vogelsang, Phys. Rev. **D70**, 034010 (2004).
- ¹¹ B.E. Bonner et al., Phys. Rev. Lett. 61, 1918 (1988); D.L. Adams et al., Phys. Lett. B261, 201 (1991); Phys. Lett. B264, 462 (1991); Z. Phys. C56, 181 (1992); A. Bravar et al., Phys. Rev. Lett. 77, 2626 (1996).
- ¹² C. Bourrely and J. Soffer, Eur. Phys. J. C36, 371 (2004).
- ¹³ A. Bravar et al. (SMC collaboration), Nucl. Phys. Proc. Suppl. 79, 520 (1999);
A. Airapetian et al. (HERMES collaboration), Phys. Rev Lett. 94, 012002 (2005).
- ¹⁴ c.f. A. Airapetian et al., Ref [13]
- ¹⁵ M. Anselmino, M. Boglione, U. D'Alesio, E. Leader, S. Melis and F. Murgia, hep-ph/0509035.
- ¹⁶ M. Boglione and E. Leader, Phys. Rev. D 61, 114001 (2000).
- ¹⁷ J. Soffer, Phys. Rev. Lett. 74, 1292 (1995).
- ¹⁸ U. d'Alesio and F. Murgia, Phys. Rev. D 70, 074009 (2004); I. Schmidt, J. Soffer, and J.-J. Yang, Phys. Lett. B612, 258 (2005).
- ¹⁹ D. Boer and W. Vogelsang, Phys. Rev. D 69, 094025 (2004).
- ²⁰ V. Guzey, M. Strikman, and W. Vogelsang, Phys. Lett. B603, 173 (2004).
- ²¹ L.C. Bland et al., Eur. Phys. J. C 43, 427 (2005) ; c.f. Ref 20.
- ²² D. Kharzeev, E. Levin, and L. McLarren, Nucl. Phys. A748, 627 (2005).
- ²³ A. Ogawa et al. (STAR Collaboration), nucl-ex/0408004.
- ²⁴ *Proposal for a Large Area Time of Flight System for STAR*, The STAR TOF Collaboration, May 24, 2004